pubs.acs.org/Biomac

Article

Safe Polycationic Dendrimers as Potent Oral In Vivo Inhibitors of *Mycobacterium tuberculosis*: A New Therapy to Take Down Tuberculosis

Serge Mignani,* Vishwa Deepak Tripathi, Dheerj Soam, Rama Pati Tripathi,* Swetarka Das, Shriya Singh, Ramakrishna Gandikota, Regis Laurent, Andrii Karpus, Anne-Marie Caminade, Anke Steinmetz, Arunava Dasgupta,* Kishore Kumar Srivastava,* and Jean-Pierre Majoral*

Cite This: *Biomacromolecules* 2021, 22, 2659−2675

Read Online

ACCESS | Metrics & More | Article Recommendations | Supporting Information

ABSTRACT: The long-term treatment of tuberculosis (TB) sometimes leads to nonadherence to treatment, resulting in multidrug-resistant (MDR) and extensively drug-resistant (XDR) tuberculosis. Inadequate bioavailability of the drug is the main factor for therapeutic failure, which leads to the development of drug-resistant cases. Therefore, there is an urgent need to design and develop novel antimycobacterial agents minimizing the period of treatment and reducing the propagation of resistance at the same time. Here, we report the development of original and noncytotoxic polycationic phosphorus dendrimers essentially of generations 0 and 1, but also of generations 2−4, with pyrrolidinium, piperidinium, and related cyclic amino groups on the surface, as new antitubercular agents active *per se*, meaning with intrinsic activity. The strategy is based on the phenotypic screening of a newly designed phosphorus dendrimer library (generations 0−4) against three bacterial strains: attenuated *Mycobacterium tuberculosis* H37Ra, virulent *M. tuberculosis* H37Rv, and *Mangora bovis* BCG. The most potent polycationic phosphorus dendrimers **1G0**,$_{HCl}$ and **2G0**,$_{HCl}$ are active against all three strains with minimum inhibitory concentrations (MICs) between 3.12 and 25.0 μg/mL. Both are irregularly shaped nanoparticles with highly mobile branches presenting a radius of gyration of 7 Å, a diameter of maximal 25 Å, and a solvent-accessible surface area of dominantly positive potential energy with very localized negative patches arising from the central N_3P_3 core, which steadily interacts with water molecules. The most interesting is **2G0**,$_{HCl}$, showing relevant efficacy against single-drug-resistant (SDR) *M. tuberculosis* H37Rv, resistant to rifampicin, isoniaid, ethambutol, or streptomycin. Importantly, **2G0**,$_{HCl}$ displayed significant in vivo efficacy based on bacterial counts in lungs of infected Balb/C mice at a dose of 50 mg/kg oral administration once a day for 2 weeks and superior efficacy in comparison to ethambutol and rifampicin. This series of polycationic phosphorus dendrimers represents first-in-class drugs to treat TB infection, could fulfill the clinical candidate pipe of this high burden of infectious disease, and play a part in addressing the continuous demand for new drugs.

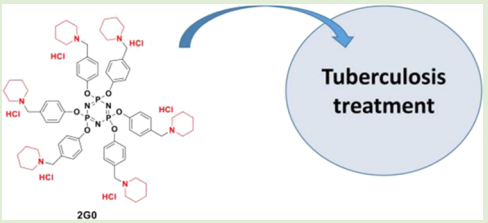

INTRODUCTION

Throughout history, the disease of tuberculosis (TB) has been known by different names: consumption, phthalmia, and white plague. Cristóbal Rojas (1857−1890) was suffering from tuberculosis and painted the famous "La Miseria" in 1886.[1] In it, he depicts the social aspect of the disease and its relationship with living conditions at the end of the 19th century. Tuberculosis (TB) is a contagious, airborne infectious disease caused most commonly by infection with various pathogen strains of mycobacteria, such as *Mycobacterium tuberculosis* (MTB), and is a major public health burden. MTB is a small aerobic nonmotile bacillus. According to the World Health Organization (WHO), an estimated 10 million people fell ill with TB in 2019. This number has been declining very slowly in recent years.[2] There were close to 1.4 million and 208 000 TB deaths among HIV-negative and HIV-coinfected patients, respectively.[2] Eight countries accounted for two-thirds of the global total: India (26%), Indonesia (8.5%), China (8.4%), the Philippines (6.0%), Pakistan (5.7%), Nigeria (4.4%), Bangladesh (3.6%), and South Africa (3.6%).[2] Despite the great reduction of incidence and mortality rate over the years, the current challenge is the increase in the prevalence of multidrug-resistant TB (MDR-TB) and extensively drug-resistant TB (XDR-TB), a form of TB that is resistant to at least four of the core anti-TB drugs since the introduction of several types of drugs. In 2016, an estimated 490 000 people worldwide developed MDR-TB.[2] Consequently, TB represents

Received: March 19, 2021
Revised: April 28, 2021
Published: May 10, 2021

https://doi.org/10.1021/acs.biomac.1c00355
Biomacromolecules 2021, 22, 2659−2675

a tough challenge and a public health threat. Moreover, according to the WHO, the recent Covid-19 pandemic threatens to reverse the progress made in recent years in the fight against tuberculosis. As a result, the countries most affected by tuberculosis are focusing more on Covid-19 detection than on TB detection. According to the WHO annual report, TB could cause 200 000−400 000 more deaths this year than the 1.4 million in 2019, despite the existence of a cure.[2]

Effective treatment is difficult due to the specific structure and chemical composition of the mycobacteria cell wall hindering the entry of drugs, which renders many drugs and antibiotics ineffective. However, the antibiotics isoniazid, rifampicin (RIF), pyrazinamide, ethambutol, and streptomycin are the major first-line pulmonary anti-TB drugs that are all typically applied as 6 month treatment.[3] The majority of anti-TB drugs are administered orally except for *Streptomycin*, *Amikacin*, *Kamamycin*, and *Capreomycin*, which are administered intravenously. Also, natural compounds with potential for the treatment of TB were recently highlighted[4] as well as vaccines.[5] Poor patient compliance to prescribed regimens and the emergence of resistant strains are the major problems during TB long-term treatment, which involves continuous, frequent multiple drug dosing. At this point, two strategies have been developed: (1) shortening the treatment duration and reducing the dosing frequency with the capacity to tackle drug-resistant TB; and (2) developing new drug formulations to reduce toxic side effects. Indeed, the introduction of long-duration drug formulations that release antimicrobial agents—incorporating both hydrophilic and hydrophobic substances—in a slow and sustained manner, allowing the reduction in frequency and total number of doses, represents an important therapeutic strategy against TB.[6] In this direction, several stable nanoparticle-based formulations for the controlled and sustained release of first-line anti-TB drugs such as isoniazid, rifampicin, and pyrazinamide have been described and show good efficiency in in vivo models. For instance, poly(lactide-*co*-glycolide) (PLG) nanoparticles, lectin-functionalized PLG nanoparticles, and solid lipid nanoparticles were developed by the oral, subcutaneous, or aerosol route of administration.[7] Recently, several nanoparticles for the delivery of anti-TB drugs directly to the lungs via the respiratory route have been analyzed. Globally speaking, the main advantages of using nanoparticles, e.g., lipids, polymers, and proteins, in inhaled anti-TB drug delivery are as follows: (1) direct drug delivery in the lung targeting alveolar macrophages; (2) decreased risk of systemic toxicity; (3) delivery of multiple drugs simultaneously; (4) shortened treatment regimen; and (5) improved patient compliance.[8] The cost of treatment, stability, and large-scale production of drug formulations are the main issues to be analyzed to bridge the gap between theory and clinical reality.[9]

Taken together, there is an urgent need for new efficacious and affordable chemotherapeutics with higher efficacy, which is the main cause for failures in clinical drug development.[10,11]

Recently, an interesting review highlighted the development of nanoparticles in TB treatment.[12] Two strategies have been developed: (1) antimycobacterial activities based on intrinsic activities; and (2) nanoparticles as nanocarriers of known antitubercular drugs for oral or pulmonary administrations. Silver, gold, iron, iron oxide, and gallium nanoparticles targeting macrophages were used in vitro and in vivo with intrinsic antimycobacterial, in addition to antibacterial activity. Achievement of biodegradable profiles is the main challenge. Several of these nanoparticles are coated, for instance, with polyacrylic acid and polysaccharide (chitosan). PLG wheat-germ agglutinin-coated PLG, poly(lactic-*co*-glycolic acid) (PLGA), chitosan, and gelatin are the main nanocarriers used, whereas rifampicin, isoniazid, pyrazinamide, and ethambutol are the main drugs for both oral and pulmonary deliveries. In addition, several surface-functionalized nanoparticles, such as gelatin, cationic lipids, and PLGA coated with mannose, lactose, mycolic acids, and PEG, with carried drugs such as isoniazid, rifampicin, and moxifloxacin were developed for antimycobacterial drug delivery.

To the best of our knowledge, no report emphasized the development of dendrimers, which can be considered as soft nanoparticles, as drug *per se* against TB. Earlier works have described the use of dendrimers as nanocarriers and have been highlighted in several reviews.[13,14] Dineshkumar et al. described the long-duration release of rifampicin-loaded PEGylated poly(amidoamine) (PAMAM) dendrimers,[15] whereas Bellini et al. showed the high stability of the rifampicin−PAMAM complex under physiological pH and the rapid release of rifampicin molecules under an acidic medium, which is similar to the acidic domains of the macrophage where the Mycobacterium resides.[16] Interestingly, Jain et al. described the intracellular macrophage uptake of rifampicin-loaded mannosylated PPI dendrimers,[17] whereas Singh et al. used the same dendrimers for delivery of isoniazid.[18] A recent review has emphasized these new ways to treat tuberculosis using dendrimers as nanocarriers.[19]

Dendrimers are three-dimensional macromolecules with a high degree of molecular uniformity and a perfectly controlled shape, surface chemistry, and size in the range of 1−15 nm. A wide range of literature about dendrimers is available today.[20] They display dendritic branches composed of hydrophobic and hydrophilic moieties radiating out from a central core unit. Interior-layer generations, G*n* (G), where *n* ranges generally from 0 to 6 and more exceptionally to 12 and even 13, are made of regularly repeating branching units attached to the core. The dendrimer diameter increases nonexponentially, whereas the number of surface groups increases exponentially for each generation. Because of their highly branched, three-dimensional architecture and versatile surface functionalization, dendrimers have been engineered for use as nanodevices, either nanocarrier drug approaches[21] or drugs *per se*,[22] as well for the construction of dendrimer hybrid materials;[23] for catalytic properties,[24] PAMAM dendrimers are the most extensively considered.[25]

For several years, Majoral, Caminade, and co-workers have developed biocompatible phosphorus dendrimers, which represent a versatile platform in drug delivery, e.g., drug and gene transfection delivery, as well as drugs themselves.[26] The high level of control that is possible over their architectural design, allowing for tunable control of sizes and shapes of cores and interiors as well as tunable surface functionality, is the main advantage of phosphorus dendrimers. Phosphorus dendrimers have been employed as drugs *per se* in different therapeutic fields as, for instance, anticancer,[27] antiprions,[28] anti-Alzheimer's,[29] anti-inflammatory agents,[30] etc. In addition, a large variety of administration routes can be used with dendrimers in general and phosphorus dendrimers in particular: intravenous, intraperitoneal, ocular, transdermal, oral, intranasal, and pulmonary routes.[31] The latter is very important in the case of TB because TB is caused by *M. tuberculosis* bacteria that most often affect the lungs.

https://doi.org/10.1021/acs.biomac.1c00355
Biomacromolecules 2021, 22, 2659−2675

Scheme 1. General Syntheses of $1G0_{,HCl}$−$5G0_{,HCl}$ Polycationic Phosphorus Dendrimers

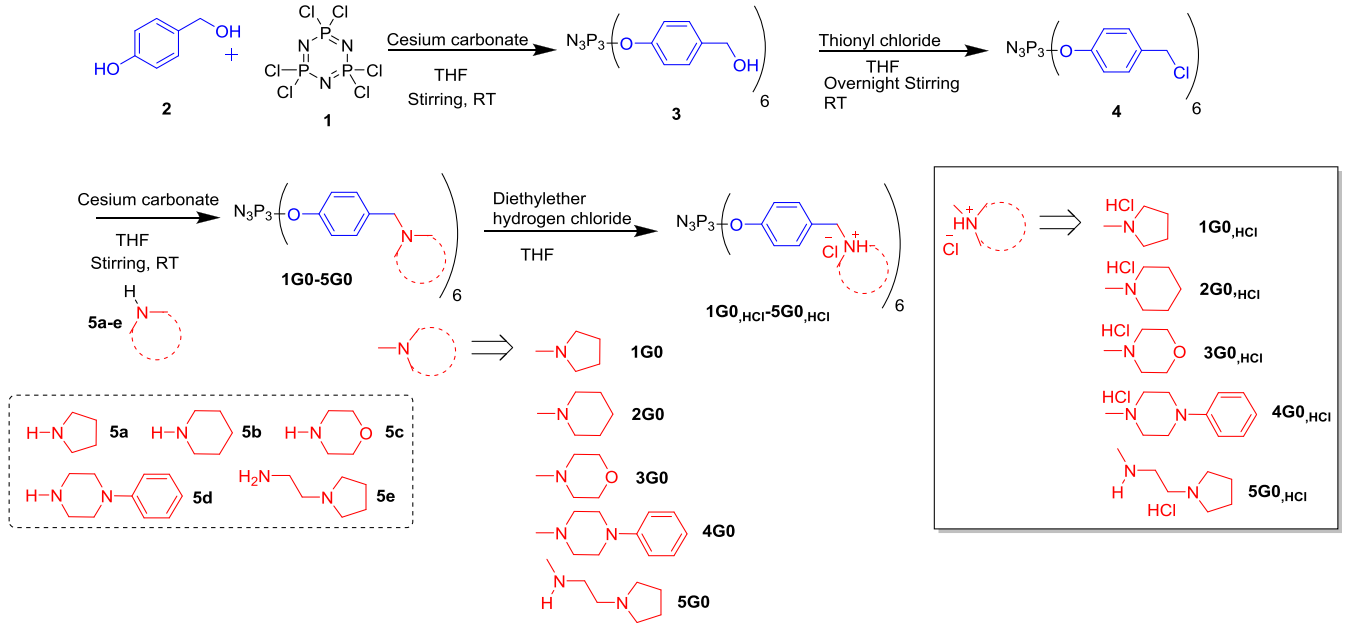

Scheme 2. General Syntheses of $6G1_{,HCl}$−$12G1_{,HCl}$ Polycationic Phosphorus Dendrimers

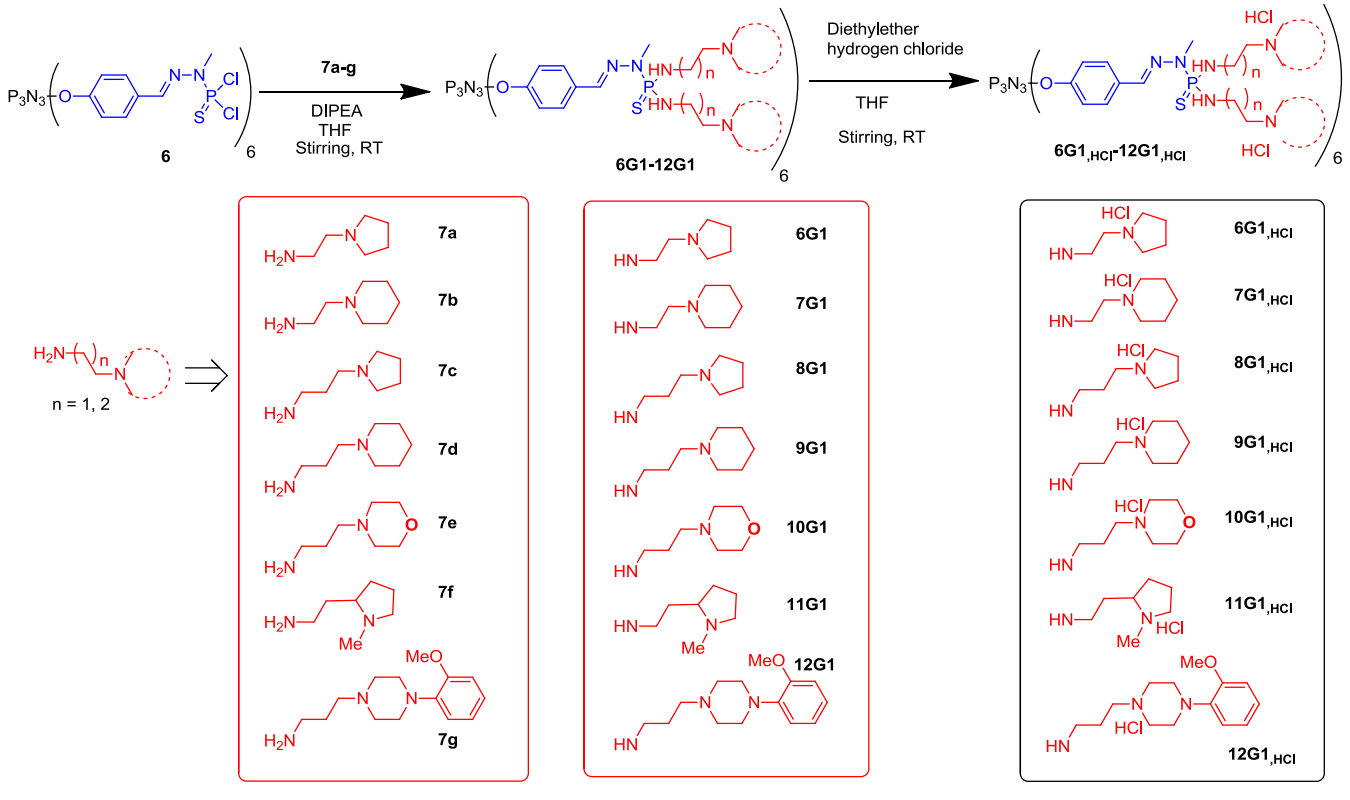

Herein, we report the development of original noncytotoxic polycationic phosphorus dendrimers as new antitubercular agents active *per se*, meaning intrinsic in vivo activity. The strategy is based on the phenotypic screening of a newly designed phosphorus dendrimer library versus, for instance, target-based[32] or fragment-based approaches.[33] These intrinsically active nanoparticles represent first-in-class drugs to treat TB infection, to fulfill the clinical candidate pipe of this high burden of infectious disease, and to play a part in addressing the continuous demand for new antitubercular drugs. We decided to develop nanoparticles in general and phosphorus dendrimers in particular due to three important points based on medical needs: (1) limited number of drugs to treat MDR-TB and XDR-TB, (2) substantial side effects including toxicity issues of drugs available, and (3) less effective second-line drugs. The antimycobacterial screening has been conducted against three bacterial strains: attenuated strain *M. tuberculosis* H37Ra, virulent *M. tuberculosis* H37Rv, and against *Mangora bovis* BCG.

https://doi.org/10.1021/acs.biomac.1c00355
Biomacromolecules 2021, 22, 2659−2675

Scheme 3. General Syntheses of 5G1 and 13G1−20G1, $5G1_{,HCl}$, and $13G_{,HCl}$−$20G1_{,HCl}$ Polycationic Phosphorus Dendrimers

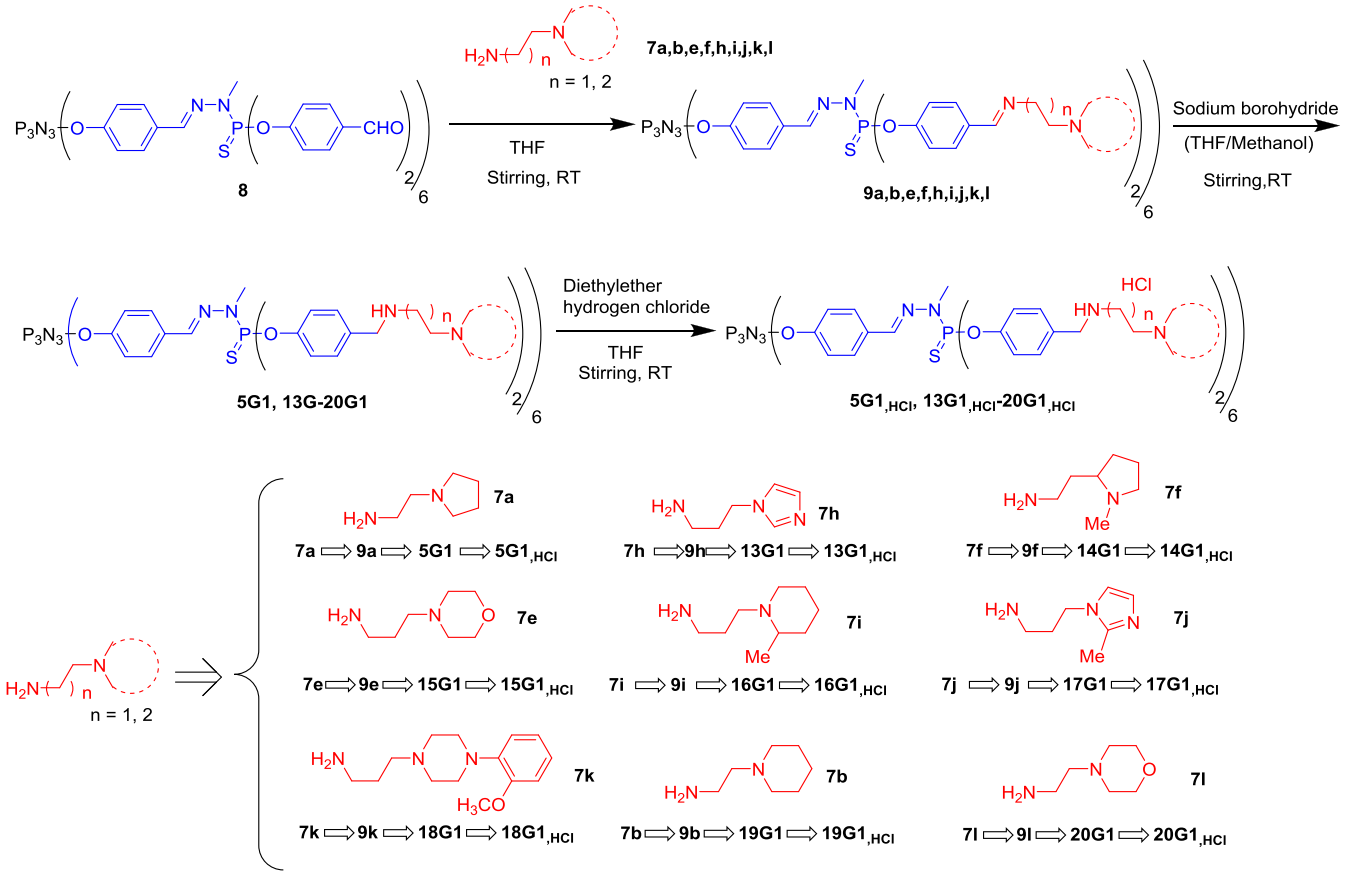

Scheme 4. General Synthesis of Dendrimers $6G2_{,HCl}$, $7G2_{,HCl}$, $6G3_{,HCl}$, $7G3_{,HCl}$, $6G4_{,HCl}$, and $7G4_{,HCl}$

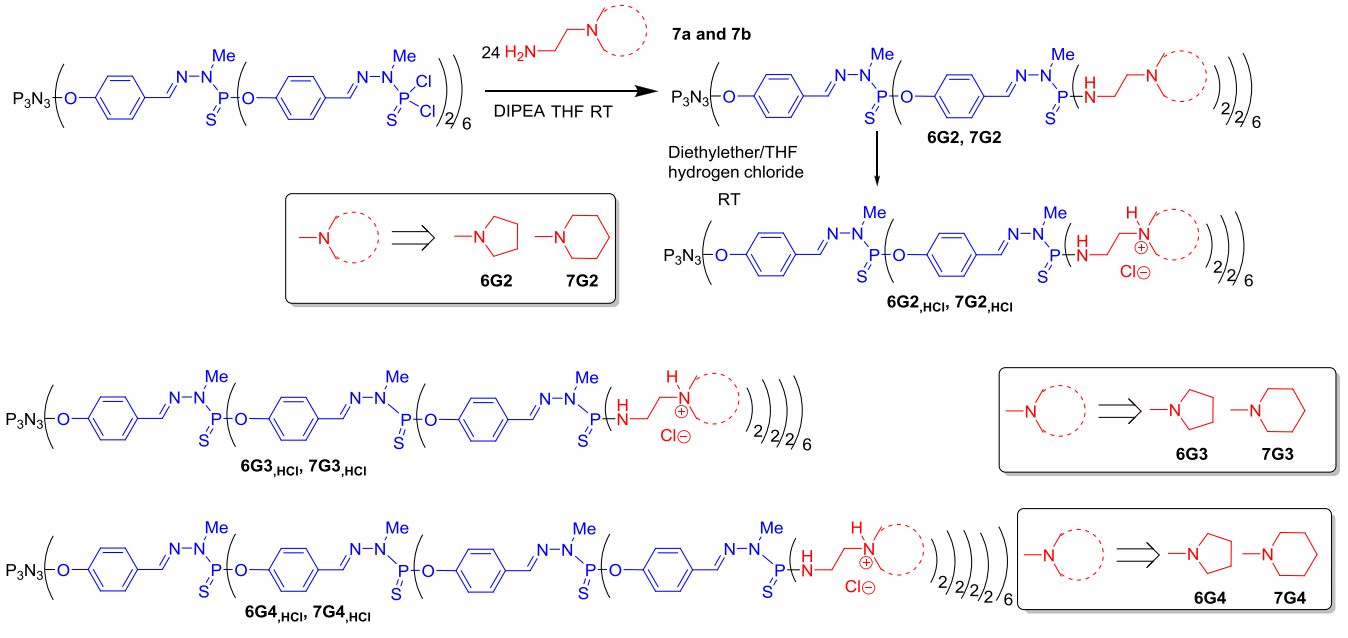

EXPERIMENTAL SECTION

Synthesis of Dendrimers. Scheme 1 shows the preparation of dendrimers of generation 0 (compounds **1G0−5G0** and of their corresponding salt). In the first step, 4-hydroxybenzyl alcohol (**2**) is grafted to the cyclotriphosphazene derivative $N_3P_3Cl_6$ in the presence of cesium carbonate at room temperature to afford compound **3**. The six benzylalcohol groups are then converted to benzylchloride **4** using thionyl chloride as the chlorinating agent,[34] which is a precursor of dendrimers **1G0−5G0**, by substitution of the chloride by diverse amines in the presence of potassium carbonate at room temperature (**5a−e**) in good yields. Finally, water-soluble compounds are obtained ($1G0_{,HCl}$−$5G0_{,HCl}$) by adding 1 equiv of HCl diethylether per terminal function (6 equiv for generation 0 compounds).

https://doi.org/10.1021/acs.biomac.1c00355
Biomacromolecules 2021, 22, 2659−2675

Scheme 2 highlights the general preparation of dendrimers of generation 1 (compounds **6G1**−**12G1** and of their respective salt). The starting point is the generation 1 dendrimer (**6**), built from the cyclotriphosphazene core.[35,36] The nucleophilic substitution with diverse primary amines (**7a**−**g**) bearing through a C_2 or C_3 linker a cyclic amine as the substituent[37] in *N*,*N*-diisopropylethylamine (DIPEA) affords in good to excellent yields the dendrimers **6G1**−**12G1**. The corresponding water-soluble compounds (**6G1**$_{,HCl}$−**12G1**$_{,HCl}$) were obtained by adding 12 equiv of HCl in diethylether to each dendrimer in quantitative yields.

Scheme 3 describes the general synthesis of dendrimers of generation 1 (compounds **5G1**, **13G1**−**20G1** and of their corresponding salt). The first step is the simple condensation reaction at room temperature between the first-generation dendrimer functionalized with 12 aldehydes (compound **8**),[30,31] with several amines **7a**, **b**, **e**, **f**, **h**, **i**, **j**, **k**, and **l** already used in Scheme 2. The second step is the reduction of the imine amines **9a**, **b**, **e**, **f**, **h**, **i**, **j**, **k**, and **l** with $NaBH_4$ at room temperature; such a reaction occurs only on the imines and not on the hydrazone linkages,[38,39] affording dendrimers **5G1** and **13G1**−**20G1** in moderate to good yields. Protonation reaction was carried out using 12 equiv of HCl per dendrimer, even if at least 24 N per dendrimer could be protonated, affording **5G1**$_{,HCl}$ and **13G**$_{,HCl}$−**20G1**$_{,HCl}$ in quantitative yield.

Scheme 4 depicts the general synthesis of dendrimers of generation 2 (compounds **6G2** and **7G2** and their respective salts), generation 3 (**6G3** and **7G3** and their respective salts), and generation 4 (**6G4** and **7G4** and their respective salts). The method of synthesis is the same as the one shown in Scheme 2, but using 24 equiv of amine for generation 2, 48 equiv for generation 3, and 96 equiv for generation 4. The water-soluble phosphorus dendrimers are obtained by adding 1 equiv of HCl per terminal function, i.e., 24 for G2, 48 for G3, and 96 for G4.

Molecular Modeling. Molecular modeling employed the Drug Discovery Suite release 2020.u2 commercialized by Schrödinger Inc executed on a Linux workstation with the CentOS7 operating system. Three-dimensional all-atom models were constructed manually in the graphical interface Maestro, energy-optimized or -minimized to convergence by programs Jaguar or Macromodel.[40,41] Conformational searches and molecular dynamics (MD) simulations were conducted by programs Macromodel and Desmond, respectively.[42] Molecular mechanics (MM) all-atom molecular force field OPLS3 with an implicit aqueous solvent and standard settings were applied unless indicated otherwise.[43] In more detail, special care was taken to construct the correct geometry of the N_3P_3 core as OPLS3 did not yield a planar conformation by MM energy minimization: cyclic $(NP(OH)_2)_3$ was quantum-mechanically energy-optimized to convergence in vacuo by the density functional theory (DFT) at the level of the B3LYP-D3 theory applying the basis set 6-31G, ** polarization, ++ diffuse basis functions, and no symmetry. Fully protonated models of **1G0** and **2G0** were derived from the optimized N_3P_3 core, the geometry of which was subsequently frozen in MM energy minimization, conformational searches, and MD simulations. Low-frequency-mode conformational searches of all rotatable, noncyclic bonds were executed for 1000 steps, minimizing every conformer for 2500 steps maximum, which only exceptionally did not yield a converged geometry. The lowest energy conformers of fully protonated **1G0** and **2G0** served to calculate solvent-accessible surfaces and their properties as well as to set up MD simulations using the explicit SPC water model at pH 7, 0.154 M NaCl, and neutralizing the system by chlorine ions. Box margins of 20 Å in all three dimensions with an optimized box orientation were applied. MD simulations were prepared and submitted via the graphical interface Maestro. Simulations on NVIDIA V100 graphical processing units (GPUs) for 1 μs as NPT ensembles at 300 K and 1 atm constraining the N_3P_3 core by weight 300 employed infinite boundary conditions, the Nose−Hoover chain thermostat, and the Martyna−Tobias−Klein barostat after standard pre-equilibration. Energy values and atomic coordinates were recorded every 25 and 250 ps, respectively. Trajectories were analyzed interactively via Maestro by calculating Simulation Interaction Diagrams, hydrogen bonds of core or branches with water molecules, radii of gyration, and radial distribution functions (rdf). Standard quality analysis showed stable simulations in terms of potential and total energy, volume, temperature, and pressure. The 1 μs simulation time sampled the conformational space well as deduced from the similar torsional distributions of equivalent rotatable bonds of the branches.

Bacterial Strains, Cell Lines, Growth Conditions, and Animals. *M. tuberculosis* H37Ra, *M. tuberculosis* H37Rv, and *M. bovis* BCG were collected from American type culture collection (ATCC). Cultures were grown in a middlebrook (MB7H9) medium supplemented with 0.2% glycerol, 0.05% tween 80, and 10% ADC. Cultures were incubated at 37 °C. The J774A.1 murine macrophage cell line and VERO cells were acquired from ATCC and cultured in an RPMI-1640 medium containing 2 mM L-glutamine, 1 mM sodium pyruvate, 4.5 g/L glucose, 1.5 g/L sodium bicarbonate, and 10 mM HEPES, supplemented with 10% heat-inactivated fetal bovine serum (FBS) at 37 °C and 5% CO_2.

Antimycobacterial Activity. Microplate Alamar Blue Assay (MABA). For the experiments, we used 96-well microplates with a flat bottom and well-grown MTB H37Ra and *M. bovis* BCG cultures of the mid-log phase (OD_{600} = 0.5−0.6) either in Sauton's medium supplemented with 3.5% glycerol and tween 80 or in MB7H9 medium. Initially, dendrimer dilutions were prepared according to their solubility, and subsequent 2-fold dilution was performed in 0.15 mL of suspension cultures in each well of the microplate. Two control wells were prepared, one containing only the suspension culture and the other containing the suspension culture plus drugs (rifampicin and streptomycin). Microplates were incubated at 37 °C for 2−3 days. After 48 h of incubation, 10% alamar blue dye solution (Resazurin 0.03%) was added to all of the wells, microplates were reincubated at 37 °C for 2−4 h, and fluorescence was measured using a spectrophotometer in the range from 530 to 590 nm.

Mycobacteria Growth Indicator Tube (MGIT) Assay. The BACTEC MGIT 960 instrument is a fully automated system that exploits the fluorescence of an oxygen sensor to detect the growth of mycobacteria in culture. The MGIT tube contains 7 mL of the modified middlebrook 7H9 broth base with OADC enrichment and PANTA, a mixture of antibiotics. For this experiment, 500 μL of MTB H37Rv cultures of the mid-log phase (OD_{600} = 0.5−0.6) was added to each MGIT tube to which dendrimers at various concentrations were added. The relative growth ratio between the drug-containing tube and the drug-free growth control (GC) tube was determined by the system's software algorithm. The final interpretation and the susceptibility results were reported by the M960 instrument automatically. The drugs from the MGIT SIRE kit were used as a positive control.

Activity against Drug-Resistant M. tuberculosis Strains. Activities of the dendrimers were determined using the MABA assay against drug-susceptible *M. tuberculosis* H37Rv ATCC 27294 (virulent tubercle bacillus), INH-resistant *M. tuberculosis* ATCC 35822 (isoniazid-resistant), RIF-resistant *M. tuberculosis* ATCC 35838 (rifapicin-resistant), STR-resistant *M. tuberculosis* ATCC 35820 (streptomycin-resistant), and ETB-resistant *M. tuberculosis* ATCC 35837 (ethambutol-resistant).

Cytotoxicity Assays. For the cytotoxicity assay, Vero cells (African green monkey kidney cell line) were added to a 96-well plate at a concentration of 4 × 10^5 cells/well in a complete RPMI medium. Vero cells were treated with dendrimers at different concentrations (10- to 12-fold of MIC) and were incubated at 37 °C with 5% CO_2 for 24 h to determine the response of dendrimer activity on cells. Two control wells, one containing only the suspension culture as a negative control and the other containing the suspension culture with ethanol as the positive control, were used. After 24 h of incubation, the 10% alamar blue dye solution (Resazurin 0.03%) was added to all of the suspension wells, microplates were reincubated at 37 °C for 2−4 h, and fluorescence was measured at 530/590 nm. The assays were done in triplicate.

Inhibition of Mycobacterial Growth and Survival in Infected J774A.1 Cells. The J774A.1 murine macrophage cell line was maintained as described previously. For infection, the J774A.1 cells

https://doi.org/10.1021/acs.biomac.1c00355
Biomacromolecules 2021, 22, 2659−2675

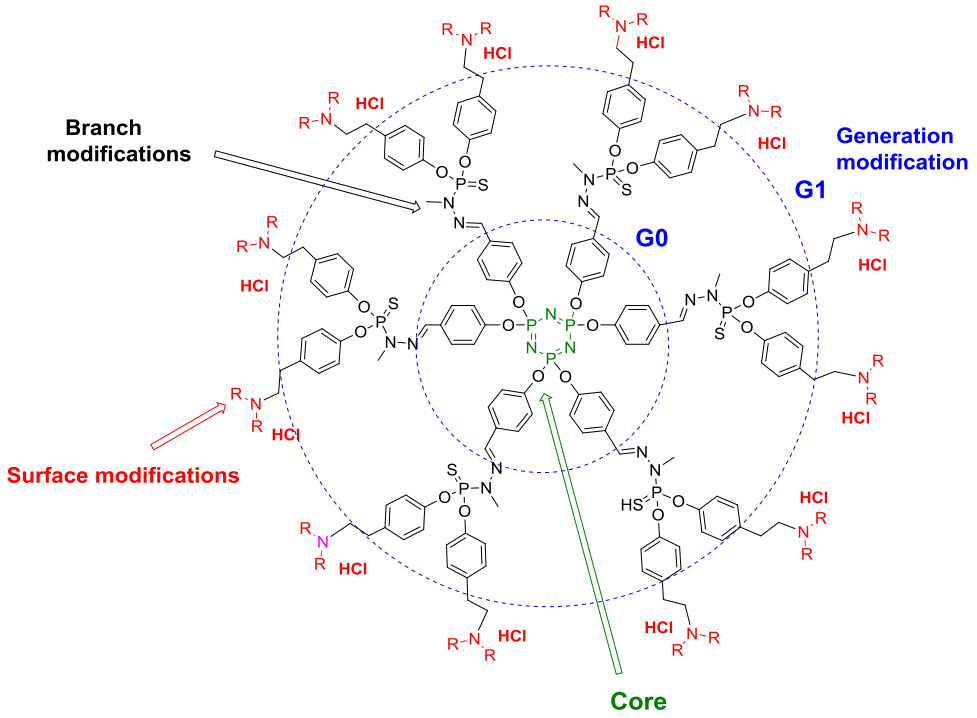

Figure 1. General 2D structure of an example of a polycationic phosphorus dendrimer.

were seeded at the density of 5×10^4 cells/well in 24-well tissue culture plates. The log-phase mycobacterial cultures were harvested by centrifugation at 2000*g* for 10 min, washed two times with sterile phosphate-buffered saline (PBS), and finally suspended in the RPMI-1640 medium. The prepared bacterial culture was added in macrophages at 1:10 MOI and allowed to undergo phagocytosis for 4 h at 37 °C and 5% CO_2. After 4 h of phagocytosis, the medium was removed and washed twice with an incomplete RPMI-1640 medium and supplemented with 100 μg/mL amikacin for 2 h for killing of extracellular mycobacteria. After 2 h of amikacin treatment, the medium was removed and washed twice with an incomplete RPMI-1640 medium. The mycobacteria H37Rv-infected J774A.1 cells were treated with dendrimers at different concentrations, and cells were incubated at 37 °C with 5% CO_2 for 48 h to determine the response of dendrimer activity on intracellular bacteria. After 48 h of dendrimer treatment, the medium was removed, and cells were washed twice with sterile PBS, and finally 0.05% sodium dodecyl sulfate (SDS) was added to lyse the cells to release the bacteria. The intracellular bacteria were calculated using BACTEC MGIT 960 systems for the detection and recovery of mycobacteria by adding 0.1 mL of harvested MTB H37Ra suspension in MGIT tubes and allow reading tubes' bar code through the BACTEC MGIT 960 system. The tubes were monitored each day for fluorescence.

Animal Experiments. Animal experiments were performed on 6-week-old BALB/c mice procured from the National Laboratory Animal Facility, CSIR-CDRI. The experimental protocols were approved by the Institutional Animal Ethics Committee.

Determination of Maximum Tolerated Dose and Toxicity of Dendrimers ***2G0,$_{HCl}$*** *in Mice.* Based on high antitubercular activities of prepared dendrimers (Tables 2−6), the most efficient compound, **2G0,$_{HCl}$**, was selected for in vivo experiments. Balb/c mice (6−7 weeks) of 20 g weight were taken and were divided into 3 groups of 3 mice each based on the given dose of **2G0,$_{HCl}$** in mice. The oral dose set (in water) for the experiment was 50 mg/kg for the first group, 33 mg/kg for the second group, and no drug (MD) in the third group. Route for the administration of the drug was kept oral, and the mice were examined daily. All of the animals in each group survived up to 3 months (100% survival after one-time daily administration during 2 weeks) and then were euthanized. In the everyday examination, we found that all mice of group one and group two showed weight loss (approximately between 2 and 4 g) of muscle mass and their behavior was found to be aggressive (data not shown).

Efficacy of ***2G0,$_{HCl}$*** *in Balb/C Mice against Mtb H37Ra.* To determine the colony-forming units (CFUs) in lungs of infected (with Mtb H37Ra) Balb/C mice, we used five groups (no drug, **2G0,$_{HCl}$** with 33 mg/kg, **2G0,$_{HCl}$** 50 mg/kg, rifampicin 10 mg/kg, and ethambutol 100 mg/kg) of Balb/C mice.

Female BALB/c mice, 5−6 weeks old, were taken for the experiment. The mice were divided into five groups (n = 5) of 6 mice in each groups. All groups were injected with MTB H37Ra intravenously. Animals were treated orally starting from seven days post infection daily for 2 weeks. After 2 weeks, all of the mice were sacrificed, and lungs and spleen were homogenized in 5 mL of normal saline, serially diluted, and plated on Middlebrook 7H11 agar plates supplemented with OADC for bacillary load detection. After incubation for 4 weeks at 37 °C, colony-forming units (CFUs) were enumerated and the data were averaged across experiments.

Statistical Analysis. Statistical analysis was performed using GraphPad Prism 6.0 software (GraphPad Software, La Jolla, CA). Comparison between three or more groups was performed using one-way analysis of variance (ANOVA), with post hoc Tukey's multiple comparison tests. P-values of <0.05 were considered to be significant.

Preliminary Mechanism of Action Studies of 2G0,$_{HCl}$. For this, a sublethal concentration of **2G0,$_{HCl}$** (1.56 μg/mL) was used to treat MTB H37Ra for 2 h. Equal amounts of whole MTB cell lysate proteins were separated by 1-DE, followed by 2-DE on 12% sodium dodecyl sulfate−polyacrylamide gel electrophoresis (SDS-PAGE), and stained with Coomassie Brilliant Blue R-250. Stained spots were cut out from the gels to process for matrix-assisted laser desorption/ionization (MALDI) mass spectrometry (MS)−MS using the standard gel digestion method with trypsin. Differently expressed proteins were identified. Three biological and technical replicates were used to derive the data.

RESULTS AND DISCUSSION

Synthesis of Dendrimers. Our strategy for synthesis was to construct an original polycationic phosphorus dendrimer library of 27 members to evaluate the influence of the cationic moieties, the nature of the branches, and the size (generations:

https://doi.org/10.1021/acs.biomac.1c00355
Biomacromolecules 2021, 22, 2659−2675

Table 1. Chemical Moieties on the Surface of Dendrimers of Generations 0 and 1 and from the Last Phosphorus Atom on the Considered Branch

Generation	Number of dendrimers prepared	Chemical moieties on the surface from the last phosphorus atom on the considered branch
G0	5	
G1	16	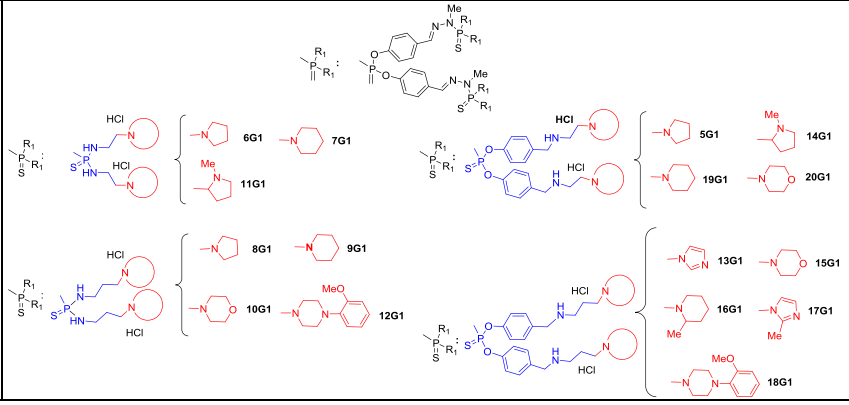

Table 2. Chemical Structure and Antitubercular Activity of Generation 0 Dendrimers[a]

S. No.	Number of amino groups on the surface	Chemical Structure	CC_{50} (Vero Cell line) (μg/mL)	Antimycobacterial Activity[a] (μg/mL)			Intracellular Activity[a] J774A.1 (μg/mL)	
				MTB H37Ra	*M. bovis* BCG	*MTB* H37Rv	*MTB* H37Ra	*MTB*H37 Rv
1G0,HCl	6	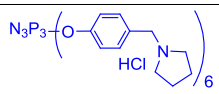	10	12.5	12.5	3.12	Inactive	Not done
2G0,HCl	6	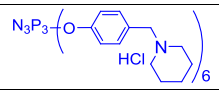	50	25	25	3.12	12.5	6.12
3G0,HCl	6	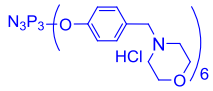	100	Inactive	Inactive	6.25	Inactive	Inactive
4G0,HCl	6	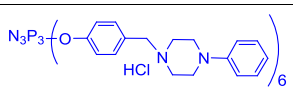	50	Inactive	Inactive	Inactive	Inactive	Not done
5G0,HCl	6	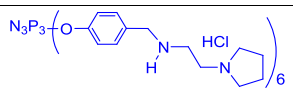	25	50	100	Inactive	Inactive	Not done

[a]The 2-fold dilutions of each compound were screened. The experiments were repeated three times.

G*n*, *n* = 0, 1, 2, 3, and 4), on their antimycobacterial activity. Figure 1 shows the general two-dimensional (2D) structure of an example of polycationic phosphorus dendrimer of generation 1.

Pyrrolidino, *N*-methyl pyrrolidino, piperidino, *N*-methyl piperidino, morpholino, imidazolino, 1-phenyl-piperazino, pyrazine-2-carbonyl, and nicotinic groups were introduced on the surface of phosphorus dendrimers to evaluate the influence of the cationic moieties on their antimycobacterial activity. Tables 1−6 represent all of the dendrimers prepared, classed by generation, and tested. The construction of these phosphorus dendrimers was also based on chemical feasibility and chemical stability, as well as their aqueous solubility. As shown in the Experimental Section and supplementary

https://doi.org/10.1021/acs.biomac.1c00355
Biomacromolecules 2021, 22, 2659−2675

Table 3. Chemical Structure and Antitubercular Activity of Generation 1 Dendrimers[a]

S. No.	Number of amino groups on the surface	Chemical Structure	CC_{50} (Vero Cell line) (μg/mL)	Antimycobacterial Activity[a] (μg/mL)			Intracellular Activity[a] J774A.1 (μg/mL)	
				MTB H37Ra	*M. bovis* BCG	*MTB* H37Rv	*MTB* H37Ra	*MTB* H37Rv
6G1,HCl	12	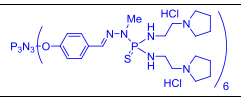	40	25	12.5	Inactive	Inactive	Not done
7G1,HCl	12	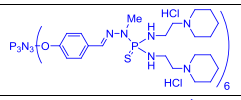	40	25	12.5	Inactive	Inactive	Not done
8G1,HCl	12	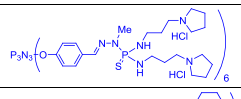	25	50	Inactive	Inactive	Inactive	Not done
9G1,HCl	12	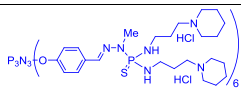	25	25	25	Inactive	Inactive	Not done
10G1,HCl	12	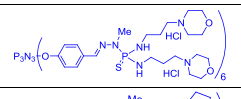	100	100	Inactive	Inactive	Inactive	Not done
11G1,HCl	12	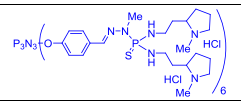	50	25	25	Inactive	Inactive	Not done
12G1,HCl	12	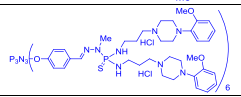	50	Inactive	Inactive	Inactive	Inactive	Not done
5G1,HCl	12	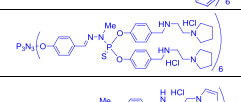	200	50	Inactive	Inactive	Inactive	Not done
13G1,HCl	12	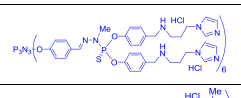	100	100	Inactive	Inactive	Inactive	Not done
14G1,HCl	12	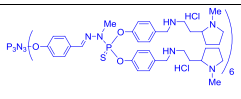	50	Inactive	Inactive	Inactive	Inactive	Not done
15G1,HCl	12	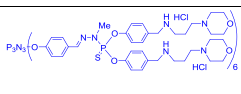	50	Inactive	Inactive	Inactive	Inactive	Not done
16G1,HCl	12	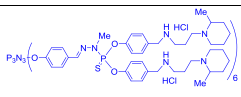	25	50	25	Inactive	Inactive	Not done
17G1,HCl	12	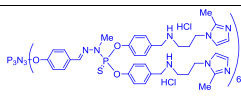	50	50	25	Inactive	Inactive	Not done
18G1,HCl	12	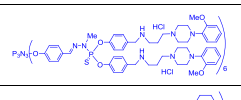	50	Inactive	Inactive	Inactive	Inactive	Not done
19G1,HCl	12	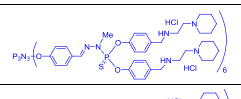	100	100	100	Inactive	Inactive	Not done
20G1,HCl	12	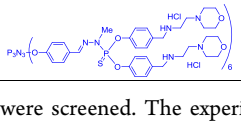	100	25	25	Inactive	Inactive	Not done

[a]The 2-fold dilutions of each compound were screened. The experiments were repeated three times.

materials, the straightforward multistep synthesis was adopted for the preparation of the phosphorus dendrimers of generation 0 (Scheme 1, compounds **1G0,HCl**–**5G0,HCl**), generation 1 (Schemes 2 and 3, compounds **5G1,HCl**–

https://doi.org/10.1021/acs.biomac.1c00355
Biomacromolecules 2021, 22, 2659−2675

Table 4. Chemical Structure and Antitubercular Activity of Generation 2 Dendrimers[a]

S. No.	Number of amino groups on the surface	Chemical Structure	CC_{50} (Vero Cell line) (μg/mL)	Antimycobacterial Activity[a] (μg/mL)			Intracellular Activity[a] J774A.1 (μg/mL)	
				MTB H37Ra	*M. bovis* BCG	*MTB* H37Rv	*MTB* H37Ra	*MTB*H37 Rv
6G2,HCl	24	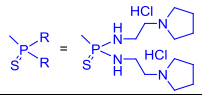	40	50	Inactive	Inactive	Inactive	Not done
7G2,HCl	24	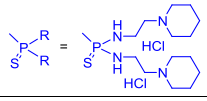	640	Inactive	Inactive	Inactive	Inactive	Not done

[a]The 2-fold dilutions of each compound were screened. The experiments were repeated three times.

Table 5. Chemical Structure and Antitubercular Activity of Generation 3 Dendrimers[a]

S. No.	Number of amino groups on the surface	Chemical structure	CC_{50} (Vero Cell Line) (μg/mL)	Antimycobacterial activity[a] (μg/mL)			Intracellular activity-J774A.1[a] (μg/mL)
				M. tub. H37Ra	*M. bovis* BCG	*M. tub.* H37Rv	
6G3,HCl	48	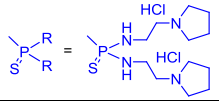	>160	>100	>100	>25	>6.25
7G3,HCl	48	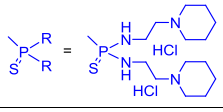	>640	>100	>100	>25	>6.25

[a]The 2-fold dilutions of each compound were screened. The experiments were repeated three times.

Table 6. Chemical Structure and Antitubercular Activity of Generation 4 Dendrimers[a]

S. No.	Number of amino groups on the surface	Chemical structure	CC_{50} (vero cell line) (μg/ml)	Antimycobacterial activity[a] (μg/ml)			Intracellular activity-J774A.1[a] (μg/ml)
				M. tub. H37Ra	*M. bovis* BCG	*M. tub.* H37Rv	
6G4,HCl	96	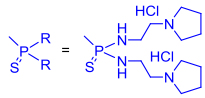	<50	>100	>100	>6.25	>6.25
7G4,HCl	96	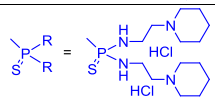	>100	>100	>100	>6.25	>6.25

[a]The 2-fold dilutions of each compound were screened. The experiments were repeated three times.

20G1,HCl), generation 2 (Scheme 4, **6G2,HCl** and **7G2,HCl**), generation 3 (Scheme 4, **6G3,HCl**, **7G3,HCl**), and generation 4 (Scheme 4, **6G4,HCl** and **7G4,HCl**). All compounds were first synthesized and characterized in the neutral form, which are named **XGn**, with X being the number of the compound and n being the generation (number of layers) of the dendrimer. The neutral dendrimers are generally less soluble in water; thus, they are protonated (with HCl) to produce their corresponding water-soluble dendrimers. These cationic dendrimers are named **XGn,HCl**.

As depicted in Schemes 1−3, first, we prepared a library of dendrimers for generation 0 (6 amino groups on the surface) and generation 1 (12 amino groups on the surface) composed of 5 and 16 functionalized dendrimers, respectively (Table 1). These dendrimers have on their surface diverse types of amino groups such as pyrrolidinium, *N*-methyl pyrrolidinium, piperidinium, *N*-methyl piperidinium, morpholinium, imidazolinium, 2-methyl-imidazolinium, 1-phenyl-piperazinium, and (2-methoxy)-1-phenyl-piperazinium. As shown in Table 1, several linker types have been introduced between the cyclotriphosphazene core ring and the diverse amino groups on the surface.

We decided to develop a phenotypic screening strategy, in contrast to the target-based strategy, although the latter has been widely used in drug discovery since the molecular biology revolution of the 1980s.[44] Indeed, the main advantages of phenotypic screens are as follows: (1) design and construction of preselected compound collections with druglike properties and optimizable chemical features to monitor efficacy and druggability, in our case, construction of a biocompatible and

https://doi.org/10.1021/acs.biomac.1c00355
Biomacromolecules 2021, 22, 2659−2675

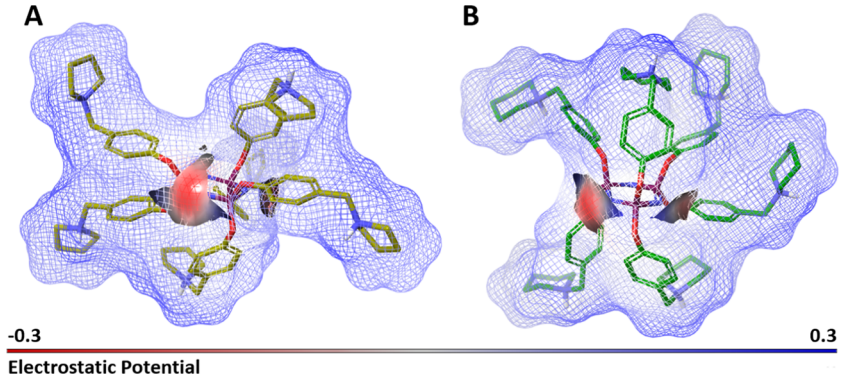

Figure 2. Three-dimensional models of fully protonated **1G0** (A) and **2G0** (B). The models are the lowest energy conformations issued from conformational searches applying an implicit solvent model. Solvent-accessible surface area (SASA) arising from the entire dendrimer or N_3P_3 core only is depicted as a mesh or solid, respectively; color ramp by potential energy from −0.3 in red over neutral in white to 0.3 in blue. The chemical structure of the dendrimers is depicted as tubes with carbon, oxygen, nitrogen, phosphor, and hydrogen atoms indicated in green, red, blue, purple, and white, respectively; nonpolar hydrogen atoms are not represented for clarity.

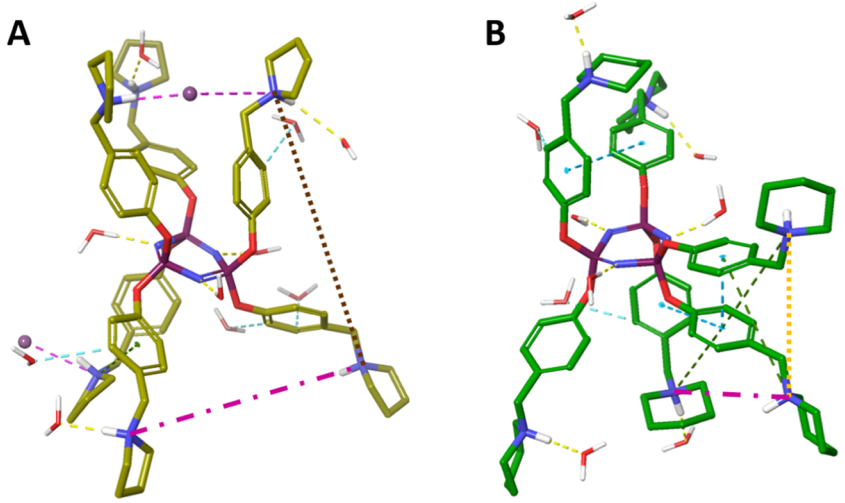

Figure 3. Snapshots of $\mathbf{1G0}_{,HCl}$ and $\mathbf{2G0}_{,HCl}$ from the molecular dynamics simulations in (A) and (B), respectively. Classical and aromatic hydrogen bonds to water, ion pairs with chlorine, parallel or perpendicular π-stacking, and cation−π interactions are indicated by dashed lines in yellow, light blue, magenta, cyan, and green, respectively. Dendrimer and water molecules are depicted in tube representation and chlorine ions as spheres colored in plum; otherwise, the color coding is as in Figure 2. Nonpolar hydrogens are not depicted for clarity. Dotted lines in orange or brown exemplarily highlight protonated tertiary amine distances giving rise to radial distribution function (rdf) maxima Max1 or Max2, respectively, in the Supporting Information Figures F9C and F10C; dash-dotted lines in magenta exemplarily indicate distances of rdf in the Supporting Information Figures F9A/B and F10A/B.

tunable phosphorus dendrimer collection within the dendrimer space;[45,46] (2) powerful assay development such as affinity, cellular profiling, and functional genomics-based approaches to screen the collections; (3) elucidation of the target(s) related to the mechanism of action by several powerful well-known technologies;[38] (4) elucidation of off-targets based on unwanted secondary phenotypes; (5) high attrition rate in the anti-infective drug discovery;[47] and (6) limited validated targets in the TB field.[32]

Based on the very interesting anti-TB activities of the protonated form of dendrimers **1G0**, **2G0**, **6G1**, **7G1**, **9G1**, **11G1**, and **20G1** (Tables 2 and 3), we decided to extend the structure−activity relationships (SAR) to the construction of libraries of generations 2 (G2, Table 4), 3 (G3, Table 5), and 4 (G4, Table 6) incorporating two phosphorus dendrimer types each. These phosphorus dendrimers have protonated pyrrolidino and piperidino moieties, which showed good anti-TB activities with dendrimers of generations 0 and 1 (Tables 2 and 3). Generations 2 and 3 are decorated on their surface with 24 or 48 protonated pyrrolidino or piperidino groups, while 96 pyrrolidinium and piperidinium groups are grafted on the surface of a dendrimer of generation 4.

Furthermore, and importantly, $\mathbf{2G0}_{,HCl}$ is stable at room temperature in an aerated aqueous solution at pH 5.5−6 for at least 9 months without any chemical degradation. This point is very important for in vivo experiments (vide infra) and potential clinical development.[48,49]

Molecular Modeling Studies. Conformational space, surface properties, and molecular dynamics of three-dimensional all-atom models of $\mathbf{1G0}_{,HCl}$ and $\mathbf{2G0}_{,HCl}$ of the developed phosphorus dendrimer library were explored by classical force-field methods. Conformational searches identified the low potential energy conformations depicted in Figure 2. Both fully protonated **1G0** and **2G0** present a solvent-accessible surface area (SASA) with very dominantly positive or neutral potential energy arising to over 85% from the branches. Very localized spots of less than 15% of the entire surface have a negative potential energy arising from solvent-

https://doi.org/10.1021/acs.biomac.1c00355
Biomacromolecules 2021, 22, 2659−2675

Table 7. Antitubercular Activity of $2G0_{,HCl}$ against Relevant Single-Drug-Resistant Mtb Strains and versus Selected Commercial Antituberculosis Drugs Rifampicin, Isoniazid, Ethambutol, and Streptomycin[a]

			MTB strain resistant to			
S. No.	compound	*M. tuberculosis* H37Rv (μg/mL)	INH (μg/mL)	RIF (μg/mL)	ETB (μg/mL)	STR (μg/mL)
1	**$2G0_{,HCl}$**	3.12	6.25	6.25	6.25	6.25
2	**$3G0_{,HCl}$**	6.25	25	12.5	25	>64
3	rifampicin	0.04	0.04	>64	0.19	0.04
4	isoniazid	0.04	>64	0.04	0.04	0.04
5	ethambutol	3.12	NT	NT	>64	0.78
6	streptomycin	1.56	NT	NT	12.5	>64

[a]RIF, rifampicin; INH, isoniaid; ETB, ethambutol; STR, streptomycin; NT, not tested.

exposed regions of the N_3P_3 core. Such surface patches give rise to hydrogen bonds formed by the core to water molecules steadily observed during molecular dynamics simulations.

These molecular dynamics simulations of **$1G0_{,HCl}$** and **$2G0_{,HCl}$** in the explicit aqueous solution evince irregularly shaped nanoparticles of changing forms with a radius of gyration of roughly 7 Å (Supporting Information Figures F5 and F6) and minimal and maximal dimensions of 14−15 Å and about 25 Å, respectively (Supporting Information Figures F7 and F8). The core typically maintains hydrogen bonds to 3 or 4 water molecules throughout the entire simulation (Supporting Information Figures F5 and F6). The protonated tertiary amines of the branches distribute rather evenly around the central N_3P_3 core (Figure 3), and their spatial distribution relative to each other is very similar for **$1G0_{,HCl}$** and **$2G0_{,HCl}$** (Supporting Information Figures F9 and F10). The nitrogen atoms tend to be at a distance of 7.5 Å when analyzing branches above or below the core and assuming conformations that extend roughly perpendicularly to the N_3P_3 plane (Supporting Information Figures F5B, F9A, and F10A,B). These conformations give rise to distances of about 14 Å when analyzing nitrogen atoms above the N_3P_3 plane with respect to those below (Supporting Information Figures F9C and F10C). Branch conformations that strongly tilt toward the N_3P_3 plane and approach nitrogen atoms of branches above and below the plane again give rise to nitrogen distances of about 7 Å (Supporting Information Figures F9C and F10C). Branch conformations are highly mobile, switching frequently from perpendicular to tilted and back, thereby distributing the positively charged nitrogen atoms evenly around the core and optimizing the electrostatic repulsion between the charged groups. Furthermore, **$1G0_{,HCl}$** and **$2G0_{,HCl}$** show numerous intramolecular interactions or form hydrogen bonds and ion pairs with solvent molecules (Figure 3). Transitory ion pairs formed with chlorine ions include two branches simultaneously binding to one chlorine ion. Classical and aromatic hydrogen bonds to water, intramolecular parallel or perpendicular π-stacking, and intramolecular cation−π interactions are also observed (Figure 3). Altogether, **$1G0_{,HCl}$** and **$2G0_{,HCl}$** show very similar molecular dynamics and globally expose the same appearance to potentially interacting macromolecules of their biological environment.

These two most potent dendrimers have a very simple structure: generation 0 bearing 6 groups on their surface, either pyrrolidinium groups (**$1G0_{,HCl}$**) or piperidinium groups (**$2G0_{,HCl}$**). They are irregularly shaped dendrimers of changing form due to highly mobile branches. Their radius of gyration is roughly 7 Å, and their minimal and maximal diameters are 14−15 and 25 Å, respectively. Their SASA is dominantly positive due to the rather evenly distributed protonated tertiary amines with localized negative spots arising from the central N_3P_3 ring. The protonated amines form transient ion pairs with chlorine in MD simulations, while the central core typically interacts with three to four water molecules. Altogether, they present a very similar appearance to macromolecules of their biological environment.

In Vitro Activity of Phosphorus Dendrimers and Their Cytotoxicity. The entire phosphorus dendrimer collection was first tested for its antimycobacterial activity against three different strains such as attenuated and virulent *M. tuberculosis* H37Ra and H37Rv, as well as *Mycobacterium bovis* BCG. The toxicity of the phosphorus dendrimers was evaluated against Vero cell lines, which were isolated from kidney epithelial cells extracted from African green monkey. All of the assays were performed in triplicate wells.

Within the generation 0 series, the antimycobacterial activities assessed as minimum inhibitory concentration (MIC) against the three strains H37Ra, BCG, and H37Rv in order are as follows: **$1G0_{,HCl}$** (MICs in μg/mL = 12.5 for Ra, 12.5 for BCG, and 3.12 for Rv), **$2G0_{,HCl}$** (MICs in μg/mL = 25.0 for Ra, 25.0 for BCG, and 3.12 for Rv), **$3G0_{,HCl}$** (MIC = 6.25 μg/mL against Rv), and **$5G0_{,HCl}$** (MICs in μg/mL = 50 for Ra and 100 for BCG) in extracellular killing of mycobacteria (Table 2). The dendrimer **$4G0_{,HCl}$** displayed no antimycobacterial activity. **$1G0_{,HCl}$** has pyrrolidinium groups on its surface, whereas **$2G0_{,HCl}$** has piperidinium groups with the same linker 4-(aminomethyl)phenoxyl moiety. The replacement of the pyrrolidinium or the piperidinium group on the surface by either a morpholinium group (compound **$3G0_{,HCl}$**) or a 4-phenyl piperidinium group (compound **$4G0_{,HCl}$**) decreases the antimycobacterial activities versus **$1G0_{,HCl}$** and **$2G0_{,HCl}$**. The increase in chain length of **$1G0_{,HCl}$**, leading to dendrimer **$5G0_{,HCl}$** with the 4-(((2-aminoethyl)amino)methyl)phenoxy chain, decreased also the antimycobacterial activities against the three strains. Interestingly, the safety index SI defined as CC_{50} against the Vero cell line divided by MICs is 16.02 versus Ra and 3.1 versus Ra for **$2G0_{,HCl}$** and **$1G0_{,HCl}$**, respectively. Table 7 shows the antitubercular activity of **$2G0_{,HCl}$** against relevant single-drug-resistant Mtb strains and versus selected commercial antituberculosis drugs such as rifampicin, isoniazid, ethambutol, and streptomycin. Very interestingly, when the activities of **$2G0_{,HCl}$** and **$3G0_{,HCl}$** were tested against SDR *M. tuberculosis*, **$2G0_{,HCl}$** was found to be active against all of the SDR strains, whereas **$3G0_{,HCl}$** demonstrated a moderate activity against rifampicin-, isoniazid-, and ethambutol-resistant H37Rv but was inactive against streptomycin-resistant H37Rv. Consequently, **$2G0_{,HCl}$** represents a particularly interesting and safe anti-TB agent based on cellular assays.

https://doi.org/10.1021/acs.biomac.1c00355
Biomacromolecules 2021, 22, 2659−2675

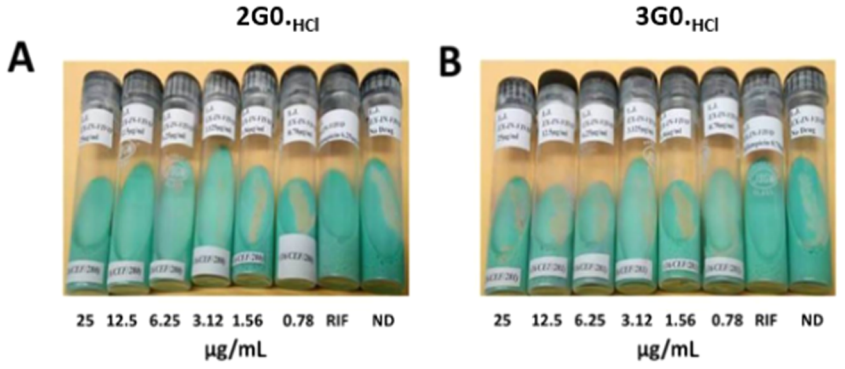

C

Sl.No	dendrimers	MIC at 6th day after incubation MTB H37Rv (µg/mL)	Cytotoxicity (CC_{50}) (µg/mL)
1	**2G0.$_{HCl}$**	6.25	50
2	**3G0.$_{HCl}$**	>25	100
3	RIFAMPICINE	0.2	ND

Figure 4. Intracellular activity of dendrimers against infected macrophages. LJ slants showing the growth of bacteria in the presence of dendrimer **2G0,$_{HCl}$** (A) and dendrimer **3G0,$_{HCl}$** (B) versus rifampicin (RIF); ND, no drug. (C) MICs and CC_{50s} of both dendrimers.

To establish additional structure−activity relationships (SARs) based on modification of generations, surface amino groups, and branches, as highlighted in Table 2, we then decided to synthesize the next generation, G1 (12 amino groups on the surface), by introducing five different types of linkers (branches) between the dendrimer core and the different amino groups on the surface: *NH*-amino-ethyl-amine (**6G1,$_{HCl}$**, **7G1,$_{HCl}$**, and **11G1,$_{HCl}$**), *NH*-amino-propyl-amine (**8G1,$_{HCl}$−10G1,$_{HCl}$** and **12G1,$_{HCl}$**), 4-(((2-aminoethyl)amino)methyl)phenoxy (**5G1,$_{HCl}$**, **14G1,$_{HCl}$,and 19G1,$_{HCl}$−20G1,$_{HCl}$**), and 4-(((2-aminopropyl)amino)-methyl)phenoxy (**13G1,$_{HCl}$** and **15G1,$_{HCl}$−18G1,$_{HCl}$**). As a general remark, several observations are apparent. All of the protonated forms of these **16G1** dendrimers displayed lower potency against the three selected strains versus dendrimers of generation 0. Within the G1 series, the most interesting G1 dendrimers are again pyrrolidinium or piperidinium groups bearing **6G1**$_{,HCl}$ and **7G1**$_{,HCl}$. However, they showed moderate antimycobacterial activities only against *MTB* H37Ra and *M. bovis* BCG with MICs of 25 and 12.5 μg/mL, respectively, similar to those of **1G0,$_{HCl}$**, **2G0,$_{HCl}$**, and **5G0,$_{HCl}$**, and no activity against *MTB* H37Rv. The phosphorus dendrimers **6G1,$_{HCl}$**, **7G1,$_{HCl}$**, and **5G0,$_{HCl}$** have the same 2-(pyrrolidin-1-yl)ethanaminium group or 2-(piperidin-1-yl)ethanaminium group on the surface. The lengthening of the chain of **6G1**$_{,HCl}$ and **7G1**$_{,HCl}$ with the same amino group on the surface decreased antimycobacterial activities, **8G1**$_{,HCl}$ versus **6G1**$_{,HCl}$ and **9G1**$_{,HCl}$ versus **7G1**$_{,HCl}$ showing MICs of ∼25−50 μg/mL. The replacement of the piperidinium group of **9G1**$_{,HCl}$ by a morpholinium group (**10G1**$_{,HCl}$) with the same linker did not improve the potency, whereas the introduction of a 1-methylpyrrolidinium group substituted in position 2 (**11G1**$_{,HCl}$) maintains moderate antimycobacterial activities only against *MTB* H37Ra and *M. bovis* BCG with an MIC of 25 μg/mL. No activity has been observed by the introduction of the (2-methoxy)-1-phenyl-piperazinium group in place of pyrrolidinium or piperidinium groups (**12G1**$_{,HCl}$ versus **8G1**$_{,HCl}$ or **9G1**$_{,HCl}$). The replacement of the *NH*-amino-ethyl-amine or the *NH*-amino-propyl-amine chains by the 4-(((2-aminoethyl)amino)methyl)phenoxy chain (**14G1**$_{,HCl}$,**19G1**$_{,HCl}$, and **20G1**$_{,HCl}$) or by the 4-(((3-aminopropyl)amino)methyl) phenoxy chain (**13G1**$_{,HCl}$, and **18G1**$_{,HCl}$) did not improve the antimycobacterial activities irrespective of the nature of the amino groups on the surface (pyrrolidinium (**6G1**$_{,HCl}$), piperidinium (**19G1**$_{,HCl}$), morpholinium (**20G1**$_{,HCl}$ and **15G1**$_{,HCl}$), imidazolinium (**13G1**$_{,HCl}$ and **17G1**$_{,HCl}$), 1-methylpyrrolidinium group substituted in position 2 (**14G1**$_{,HCl}$), 2-methylpiperidinium (**16G1**$_{,HCl}$), and (2-methoxy)-1-phenyl-piperazinium (**18G1**$_{,HCl}$) groups). For generation 1, in contrast to generation 0, no effect of the nature of the amino groups on the surface has been clearly demonstrated. All of the dendrimers showed moderate to no antimycobacterial activities. To summarize, the most relevant G1 dendrimers are **6G1**$_{,HCl}$ and **7G1**$_{,HCl}$ with the shorter chain (*NH*-amino-ethyl-amine) and the pyrrolidinium and piperidinium groups on the surface.

Based on the very interesting results for **1G0**, **2G0**, **6G1**, and **7G1**, we decided to construct a series of six dendrimers of generations 2, 3, and 4 bearing on the surface only the pyrrolidinium and piperidinium groups (Tables 4−6) on the surface. The dendrimers **6G2,$_{HCl}$** and **7G2,$_{HCl}$**, **6G3,$_{HCl}$** and **7G3,$_{HCl}$**, and **6G4,$_{HCl}$** and **7G4,$_{HCl}$** showed no antimycobacterial activities against all three strains, except for **6G2,$_{HCl}$** showing poor anti-TB activities against only *MTB* H37Ra with an MIC of 50 μg/mL but an SI of 0.8.

Interestingly, **2G0,$_{HCl}$** inhibited the mycobacterial growth and intracellular survival in infected J774A.1 cells. **2G0,$_{HCl}$** showed extracellular killing of MTB H37Rv with an MIC of 6.12 μg/mL. To assure the effect of dendrimers on intracellular replicating mycobacteria, we tested the dendrimers **2G0,$_{HCl}$** and **3G0,$_{HCl}$**. The effect of dendrimer **1G0,$_{HCl}$** on intracellularly replicating bacteria was not determined due to its low CC_{50}. For analysis of the effect of dendrimers on intracellular bacteria, we infected J774A.1 cells with MTB H37Rv and treated with different concentrations of dendrimers ranging from 0.78 to 25 μg/mL. After 48 h post infection, the cells

https://doi.org/10.1021/acs.biomac.1c00355
Biomacromolecules 2021, 22, 2659−2675

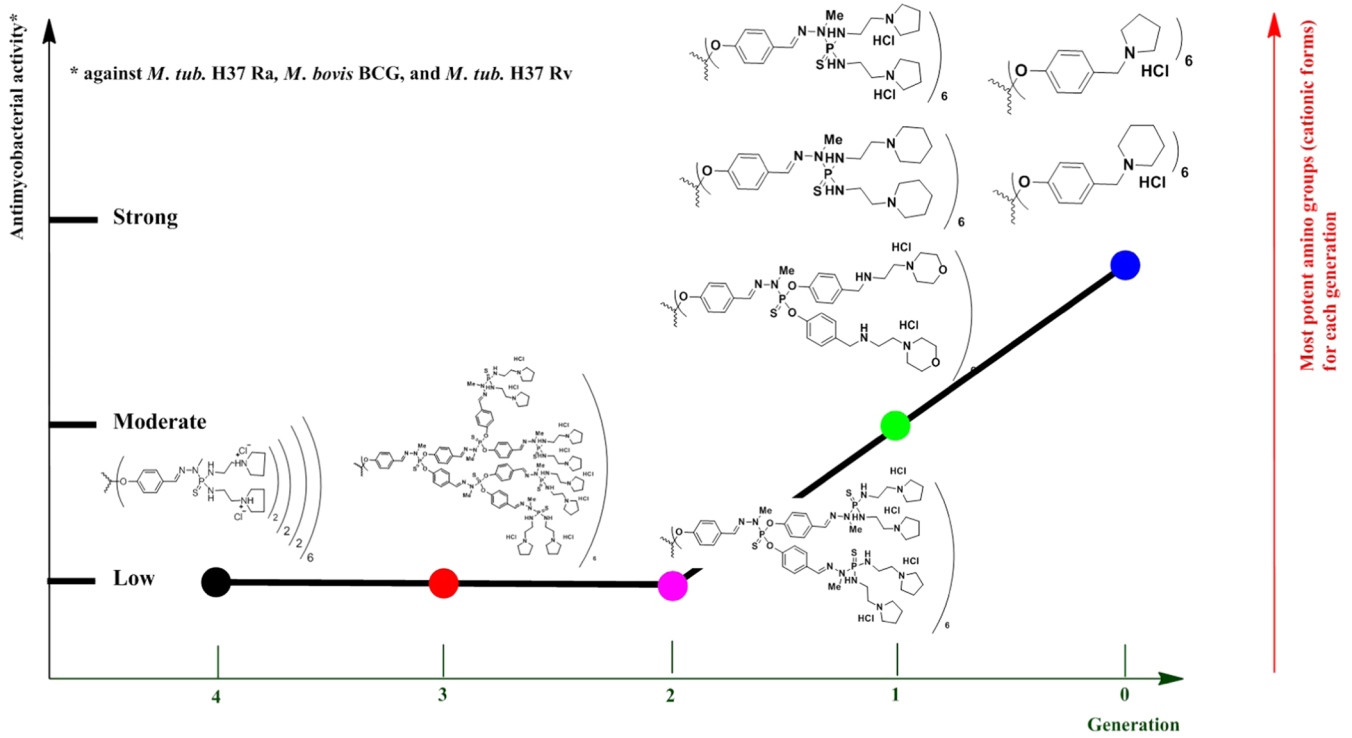

Figure 5. Main structure−activity relationships between the generation of dendrimers and antimycobacterial activities.

were harvested and added to the intracellular bacteria on LJ slants from treated and untreated cells. As shown in Figure 4, after 4−5 weeks of incubation, the colony-forming units (CFUs) were calculated, and it was observed that the MTB-infected cells treated with **2G0,**$_{HCl}$ showed no intracellular bacteria at concentrations above 6.25 μg/mL. The dendrimer **3G0,**$_{HCl}$ exhibited a marginal effect on intracellularly replicating MTB H37Rv. In these assays, rifampicin was used as a positive control.

Specificity of Active Dendrimers. To determine their antimicrobial specificity, activities of **2G0,**$_{HCl}$ and **3G0,**$_{HCl}$ were also determined against an ESKAPE panel consisting of *Escherichia coli* ATCC 25922, *Staphylococcus aureus* ATCC 29213, *Klebsiella pneumoniae* BAA-1705, *Acinetobacter baumannii* BAA-1605, and *Pseudomonas aeruginosa* ATCC 27853, where both were found to be completely inactive, with MIC evaluation indicating that their antimicrobial activity is *Mycobacterium*-specific.

As a general statement, the size of dendrimers as well as the nature of the terminal group plays key roles. Dendrimers of generation 0 bearing pyrrolidinium or piperidinium groups displayed good antimycobacterial activities against the three selected strains. In this direction, moderate biological activities were observed with generation 1 only with the shorter chain and also with the pyrrolidinium and piperidinium groups on the surface. Figure 5 represents the principal SARs among the prepared dendrimers between the generation of dendrimers and the antimycobacterial activities.

Taken together, these results fully confirm the interest of **2G0,**$_{HCl}$ as a safe antitubercular agent active against resistant strains. Consequently, **2G0,**$_{HCl}$ was tested in an animal model through oral administration.

Efficacy of 2G0,$_{HCl}$ **in Balb/C Mice against Mtb H37Ra.** Since **2G0,**$_{HCl}$ demonstrated safe and potent in vitro antimycobacterial activity, we decided to evaluate its in vivo efficacy in Balb/C mice. Two weeks of oral treatment with 33 mg/kg **2G0,**$_{HCl}$ (one-time-daily administration) reduced the mean bacterial counts in lungs of infected mice significantly by 1.0 $\log_{10}$, while 50 mg/kg **2G0,**$_{HCl}$ reduced bacterial counts by ~1.5 $\log_{10}$ as compared to the untreated group. This outcome is even better compared to rifampicin-treated groups, which is not the case at the dose of RIF of 25 mg/kg versus **2G0.**$_{HCl}$ at 33 mg/kg. Taken together, this important experiment demonstrates the superior efficacy of **2G0,**$_{HCl}$ in clearing infection from various animal tissues in comparison to ethambutol and rifampicin (Figure 6). **2G0**$_{HCl}$ is considered a very interesting lead to be optimized to improve its in vivo efficiency.

Mechanism of Action Studies of 2G0,$_{HCl}$**: Preliminary Investigations.** Since **2G0,**$_{HCl}$ demonstrated good in vitro, ex vivo, and in vivo activities, it was imperative to elucidate the mechanism of action by which killing of *MTB* H37Rv is facilitated. MALDI MS−MS data showed differential regulation of 15 specific proteins, which have been shown in Table 8 and Figure 7. In these preliminary investigational assays, we did not quantify the amount of proteins. The aim is only to evaluate the upregulation and the downregulation of proteins.

Within the 12 proteins observed, three were upregulated, namely, SodA (Fe), unnamed Gi15607825 Rv0685, and elongation factor TU Rv0685. Another 9 were downregulated, namely, GAPDH Rv1436, alkyl hydroperoxidase reductase subunit-c Rv2428, DnaK Rv0350, hypothetical protein Rv0020c, Rv2145c, phosphopyruvatehydratage, DNA-directed RNA polymerase α subunit, malate dehydrogenase, flavoprotein α subunit, and two-component response regulator protein MprA. Detailed functional characterization of differentially expressed proteins is required to identify the exact mechanism of action of the dendrimers.

https://doi.org/10.1021/acs.biomac.1c00355
Biomacromolecules 2021, 22, 2659−2675

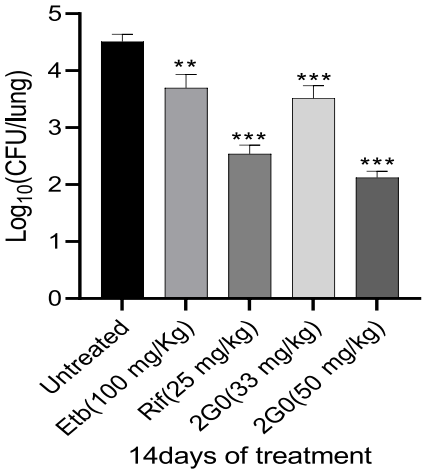

Figure 6. In vivo efficacy of $\mathbf{2G0}_{,HCl}$ in Balb/C mice. Mean $\log_{10}$ CFU/mL in lungs of mice after 14 days post treatment with $\mathbf{2G0}_{,HCl}$ (oral administration, once daily during 2 weeks), rifampicin, and ethambutol. Six mice per group were infected intravenously with $\sim 10^6$ CFU of *M. tuberculosis* H37Ra and treatment was started 7 days post infection.

CONCLUSIONS AND PERSPECTIVES

TB is an old infectious disease mainly affecting the lungs caused by *M. tuberculosis*. Compared with other diseases, TB is one of the most important killers, and TB medication can be toxic to the liver. In addition, most of the TB drugs are, in fact, bioprecursor-type prodrugs.[50] Development of MDR- and XDR-TB warrants the introduction of new chemotherapeutic tools in the arsenal of anti-TB drugs. Consequently, the search for original anti-TB derivatives with a broad spectrum and with a new scaffold is even more pertinent today. Very interestingly, we developed original anti-TB compounds based on biocompatible polycationic phosphorus dendrimers. These nanoparticles open new avenues in the tuberculosis domain and are chemically totally different from and not related to the standard anti-TB drugs. Molecular modeling studies showed that $\mathbf{1G0}_{,HCl}$ and $\mathbf{2G0}_{,HCl}$ have a radius of gyration of 7 Å and minimal and maximal diameters of 14−15 and 25 Å, respectively. Their SASA is dominantly positive due to the rather evenly distributed protonated tertiary amines with localized negative spots arising from the central N3P3 ring. The protonated amines form transient ion pairs with chlorine in MD simulations, while the central core typically interacts with three to four water molecules. $\mathbf{1G0}_{,HCl}$ and $\mathbf{2G0}_{,HCl}$ are active against three different strains, such as attenuated *M. tuberculosis H37Ra*, virulent *M. tuberculosis H37Rv*, and *Mycobacterium bovis BCG*. Importantly, the safety index values are 16.02 and 3.1 versus Ra for $\mathbf{2G0}_{,HCl}$ and $\mathbf{1G0}_{,HCl}$, respectively. Very interestingly, $\mathbf{2G0}_{,HCl}$ was tested against single-drug-resistant *M. tuberculosis* and multiple strain resistant to rifampicin, isoniazid, ethambutol, or streptomycin. $\mathbf{2G0}_{,HCl}$ showed activity against all single-drug-resistant strains, which indicates that the dendrimers possess a potential new mode of action. Moreover, our preliminary studies on their mechanism of action suggested that $\mathbf{2G0}_{,HCl}$ acts on novel targets and/or pathways. In addition, $\mathbf{2G0}_{,HCl}$ inhibited the mycobacterial growth and intracellular survival in infected J774A.1 cells. Consequently, $\mathbf{2G0}_{,HCl}$ represents a very interesting and safe anti-TB agent and was selected for in vivo experiments. A single daily oral administration for a fortnight with 50 mg/kg $\mathbf{2G0}_{,HCl}$ very significantly reduces the mean bacterial count in the lungs of infected mice by about 1.5 log10 compared to the untreated group. This bacterial reduction is greater than that observed in the rifampicin- and ethambutol-treated groups.

Taken together, all of the in vitro, in cellular, ex vivo, and in vivo experiments demonstrated that the safe and chemically stable G0 polycationic phosphorus dendrimer named $\mathbf{2G0}_{,HCl}$ represents a new chemical entity to tackle tuberculosis. Moreover, $\mathbf{2G0}_{,HCl}$ is chemically stable for up to 9 months in aerated aqueous solution, which is one of the critical points for potential clinical development. Interestingly, these original phosphorus dendrimers should be developed in combination

Table 8. List of MTB Proteins and Their Functions

identified proteins	expression level of proteins	role in MTB
SodA (Fe)	upregulation	TB leads to increased oxidative burden (ROS, RNI) in the lung that aids in the activation of TB prodrugs
		SodA (Fe) destroys radicals, which are normally produced within the cells and are toxic to biological systems ($O_2^{\bullet -} \rightarrow H_2O_2$)
unnamed Gi15607825 Rv0685	upregulation	promotes GTP-dependent binding of aminoacyl-tRNA to the A-site of ribosomes during protein biosynthesis
elongation factor TU Rv0685	upregulation	promotes GTP-dependent binding of aminoacyl-tRNA to the A-site of ribosomes during protein biosynthesis
GAPDH Rv1436	downregulation	involved in the second phase of glycolysis
alkyl hydroperoxidase reductase subunit-c Rv2428	downregulation	involved in oxidative stress response
DnaK Rv0350	downregulation	acts as a chaperone; involved in induction by stress conditions, e.g., heat shock; possibly has an ATPase activity
hypothetical protein Rv0020c	downregulation	signal transduction
Rv2145c	downregulation	cell division
phosphopyruvatehydratase	downregulation	anchorless surface-exposed proteins that bind to plasminogen
DNA-directed RNA polymerase α subunit	downregulation	DNA-dependent RNA polymerase catalyzes the transcription of DNA into RNA
malate dehydrogenase	downregulation	involved in the conversion of malate to oxaloacetate
flavoprotein α subunit	downregulation	the electron-transfer flavoprotein serves as a specific electron acceptor for other dehydrogenases
two-component response regulator protein MprA	downregulation	regulator, part of a two-component regulatory system

https://doi.org/10.1021/acs.biomac.1c00355
Biomacromolecules 2021, 22, 2659−2675

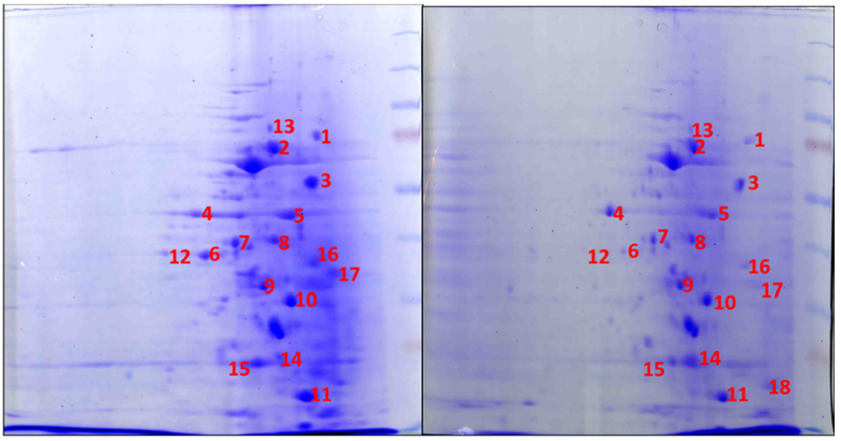

Figure 7. Two-dimensional (2D) gel profile of MTB H37Ra treated with **2G0**$_{,HCl}$.

therapy (multidrug regimens) to treat TB, for instance, with isoniazid, rifampicin, or delamanid, which are currently used. The objective is to increase treatment efficacy while avoiding resistance (MDR-TB and XDR-TB).[51] We are convinced that the main goals concerning the development of new TB drugs are to (1) reduce the duration of treatment, (2) effectively treat MDR-TB, and (3) provide treatment for patients with latent TB infection. Our original results may open new perspectives in these challenging fields.

■ ASSOCIATED CONTENT

Supporting Information

The Supporting Information is available free of charge at https://pubs.acs.org/doi/10.1021/acs.biomac.1c00355.

Preparation and characterization of compounds of generation 0: **1G0**, **2G0**, **3G0**, **5G0**, **1G0**$_{,HCl}$, **2G0**$_{,HCl}$, **3G0**$_{,HCl}$, and **5G0**$_{,HCl}$; generation 1: **5G1**, **6G1**, **7G1**, **8G1**, **9G1**, **10G1**, **11G1**, **12G1**, **13G1**, **14G1**, **15G1**, **17G1**, **18G1**, **19G**, **20G1**, **5G1**$_{,HCl}$, **6G1**$_{,HCl}$, **7G1**$_{,HCl}$, **8G1**$_{,HCl}$, **9G1**$_{,HCl}$, **10G1**$_{,HCl}$, **11G1**$_{,HCl}$, **12G1**$_{,HCl}$, **13G1**$_{,HCl}$, **14G1**$_{,HCl}$, **15G1**$_{,HCl}$, **17G1**$_{,HCl}$, **18G1**$_{,HCl}$, **19G1**$_{,HCl}$, and **20G1**$_{,HCl}$; detailed characterization of 1G0$_{,HCl}$ and **2G0**$_{,HCl}$ by NMR (^{1}**H**, ^{31}**P**),^{13}**C**{^{1}**H**},^{13}**C**-{^{31}**P**}, 2D,^{13}C,JMOD, 2D,^{13}C HMBC, 2D, and^{13}C HMQC; detailed characterization of **1G0**$_{,HCl}$ and **2G0**$_{,HCl}$ by NMR (^{1}H, ^{31}P),^{13}C{^{1}H},^{13}C{^{31}P}, 2D,^{13}C,JMOD, 2D,^{13}C HMBC, 2D, and ^{13}C HMQC, which also corroborate the full protonation of the terminal pyrrolidine or piperidine end groups; figures and statistics of noncovalent interaction counts, radii of gyration, and radial distribution functions observed by molecular dynamics simulations of **1G0**$_{,HCl}$ and **2G0**$_{,HCl}$ (PDF)

■ AUTHOR INFORMATION

Corresponding Authors

Serge Mignani − *Laboratoire de Chimie et de Biochimie Pharmacologiques et Toxicologique, PRES Sorbonne Paris Cité, CNRS UMR 860, Université Paris Descartes, 75006 Paris, France; CQM—Centro de Química da Madeira, MMRG, Universidade da Madeira, 9020-105 Funchal, Portugal*; Email: serge.mignani@paris, serge.mignani@staff.uma.pt

Rama Pati Tripathi − *Medicinal and Process Chemistry Division, CSIR-CDRI, 226031 Lucknow, India*; orcid.org/0000-0002-9256-3112; Email: rpt.cdri@gmail.com

Arunava Dasgupta − *Microbiology Division, CSIR-Central Drug Research Institute, 226031 Lucknow, India*; Email: a.dasgupta@cdri.res.in

Kishore Kumar Srivastava − *Microbiology Division, CSIR-Central Drug Research Institute, 226031 Lucknow, India*; Email: kishore@cdri.res.in

Jean-Pierre Majoral − *Laboratoire de Chimie de Coordination du CNRS, 31077 Toulouse, France; LCC-CNRS, Université de Toulouse, CNRS, 31400 Toulouse, France*; orcid.org/0000-0002-0971-817X; Email: jean-pierre.majoral@lcc-toulouse.fr

Authors

Vishwa Deepak Tripathi − *Laboratoire de Chimie de Coordination du CNRS, 31077 Toulouse, France; LCC-CNRS, Université de Toulouse, CNRS, 31400 Toulouse, France*

Dheerj Soam − *Microbiology Division, CSIR-Central Drug Research Institute, 226031 Lucknow, India*

Swetarka Das − *Microbiology Division, CSIR-Central Drug Research Institute, 226031 Lucknow, India*

Shriya Singh − *Microbiology Division, CSIR-Central Drug Research Institute, 226031 Lucknow, India*

Ramakrishna Gandikota − *Laboratoire de Chimie de Coordination du CNRS, 31077 Toulouse, France; LCC-CNRS, Université de Toulouse, CNRS, 31400 Toulouse, France*

Regis Laurent − *Laboratoire de Chimie de Coordination du CNRS, 31077 Toulouse, France; LCC-CNRS, Université de Toulouse, CNRS, 31400 Toulouse, France*

Andrii Karpus − *Laboratoire de Chimie de Coordination du CNRS, 31077 Toulouse, France; LCC-CNRS, Université de Toulouse, CNRS, 31400 Toulouse, France*; orcid.org/0000-0002-5760-3086

Anne-Marie Caminade − *Laboratoire de Chimie de Coordination du CNRS, 31077 Toulouse, France; LCC-CNRS, Université de Toulouse, CNRS, 31400 Toulouse, France*

https://doi.org/10.1021/acs.biomac.1c00355
Biomacromolecules 2021, 22, 2659−2675

Anke Steinmetz − *Sanofi R&D, Integrated Drug Discovery, Centre de Recherche Vitry-Alfortville, 94403 Vitry-sur-Seine Cedex, France*

Complete contact information is available at: https://pubs.acs.org/10.1021/acs.biomac.1c00355

Author Contributions

All of the other coauthors contributed equally. The authors declare the following competing financial interest(s): A.S. is a Sanofi employee and may hold shares and/or stock options in the company.

Notes

The authors declare no competing financial interest.

■ ACKNOWLEDGMENTS

We thank the Director CSIR-CDRI for the support. S.M. acknowledges the support of FCT-Fundacao para a Ciencia e a Tecnologia (project PEst-OE/QUI/UI0674/2013, CQM, Portuguese Government funds) and ARDITI through the project M1420-01-0145-FEDER-000005—Centro de Quimica da Madeira—CQM+ (Madeira 14-20), and J.-P.M., A.-M.C. R.L., and A.K. acknowledge the funds from Centre National de la Recherche Scientifique (CNRS, France). The work was funded through the Indo-French (CEFIPRA) project CEFI-PRA-5303-2. This manuscript bears CSIR-CDRI communication number 10240.

■ REFERENCES

(1) Wikipedia. History of Tuberculosis, 2021. https://en.wikipedia.org/wiki/History_of_tuberculosis#/media/File:Cristobal_Rojas_37a.JPG.

(2) World Health Organization, G.S.. Global Tuberculosis Report, 2020. https://apps.who.int/iris/bitstream/handle/10665/336069/9789240013131-eng.pdf.

(3) Kendall, E. A.; Azman, A. S.; Cobelens, F. G. MDR-TB treatment as prevention: The projected population-level impact of expanded treatment for multidrug-resistant tuberculosis. *PLoS One* **2017**, *12*, No. e0172748.

(4) Maiolini, M.; Gause, S.; Taylor, J.; Steakin, T.; Shipp, G.; Lamichhane, P.; Deshmukh, B.; Shinde, V.; Bishayee, A.; Deshmukh, R. R. The War against Tuberculosis: A Review of Natural Compounds and Their Derivatives. *Molecules* **2020**, *25*, No. 3011.

(5) Mascola, J. R.; Fauci, A. S. Novel vaccine technologies for the 21st century. *Nat. Rev. Immunol.* **2020**, *20*, 87−88.

(6) Moodley, R.; Godec, T. R. STREAM., o. b. o. t., Trial Team. Short-course treatment for multidrug-resistant tuberculosis: the STREAM trials. *Eur. Respir. Rev.* **2016**, *25*, 29−35.

(7) Gelperina, S.; Kisich, K.; Iseman, M. D.; Heifets, L. The Potential advantages of nanoparticle drug delivery systems in chemotherapy of tuberculosis. *Am. J. Respir. Crit. Care Med.* **2005**, *172*, 1487−1490.

(8) Jawahar, N.; Reddy, G. Nanoparticles: A novel pulmonary drug delivery system for tuberculosis. *J. Pharm. Sci. Res.* **2012**, *4*, 1901−1906.

(9) Mignani, S.; Rodrigues, J.; Tomas, H.; Roy, R.; Shi, X.; Majoral, J.-P. Bench-to-bedside translation of dendrimers: Reality or utopia? A concise analysis. *Adv. Drug Delivery Rev.* **2018**, *136*−*137*, 73−81.

(10) Arrowsmith, J. Trial watch: Phase II failures: 2008−2010. *Nat. Rev. Drug Discovery* **2011**, *10*, 328−329.

(11) Hay, M.; Thomas, D. W.; Craighead, J. L.; Economides, C.; Rosenthal, J. Clinical development success rates for investigational drugs. *Nat. Biotechnol.* **2014**, *32*, 40−51.

(12) Costa-Gouveia, J.; Aınsa, J. A.; Brodin, P.; Lucıa, A. How can nanoparticles contribute to antituberculosis therapy? *Drug Discovery Today* **2017**, *22*, 600−607.

(13) Pati, K.; Bagade, S.; Bonde, S.; Sharma, S.; Saraogi, G. Recent therapeutic approaches for the management of tuberculosis: Challenges and opportunities. *Biomed. Pharmacother.* **2018**, *99*, 735−745.

(14) Skwarecki, A. S.; Milewskib, S.; Schielmann, M.; Milewska, M. J. Antimicrobial molecular nanocarrier-drug conjugates. *Nanomedicine* **2016**, *12*, 2215−2240.

(15) Dineshkumar, P.; Panneerselvam, T.; Selvaraj, K. K.; Kumar, P. V. Formulation of rifampicin loaded PEGylated 5.0G EDA-PAMAM dendrimers as effective long-duration release drug carriers. *Curr. Drug Ther.* **2017**, *12*, 115−126.

(16) Bellini, G. R.; Guimar, A. P.; Pachecoa, M. A. C.; Diasa, D. A.; Furtadoc, V. R.; de Alencastro, R. B.; Hortac, B. A. C. Association of the anti-tuberculosis drug rifampicin with PAMAM dendrimer. *J. Mol. Graphics Modell.* **2015**, *60*, 34−42.

(17) Kumar, P. V.; Asthana, A.; Dutta, T.; Jain, N. K. Intracellular macrophage uptake of rifampicin loaded mannosylated dendrimers. *J. Drug Targeting* **2006**, *14*, 546−556.

(18) Singh, N.; Gautam, S. P.; Singh, H. L.; Dhiman, A.; Siddiqui, G.; Verma, A. Isoniazid loaded dendrimer based nano carriers for the delivery of anti-tuberculosis. *Indian Res. J. Pharm. Sci.* **2016**, *3*, 519−529.

(19) Mignani, S.; Tripathi, R. P.; Chen, L.; Caminade, A.-M.; Shi, X.; Majoral, J.-P. New ways to treat tuberculosis using dendrimers as nanocarriers. *Pharmaceutics* **2018**, *10*, No. 105.

(20) Chis, A. A.; Dobrea, C.; Morgovan, C.; Arseniu, A. M.; Rus, L. L.; Butuca, A.; Juncan, A. M.; Totan, M.; Vonica-Tincu, A. L.; Cormos, G.; Muntean, A. C.; Muresan, M. L.; Gligor, F. G.; Frum, A. Applications and Limitations of Dendrimers in Biomedicine. *Molecules* **2020**, *25*, No. 3982.

(21) Madaan, K.; Kumar, S.; Poonia, N.; Lather, V.; Pandita, D. Dendrimers in drug delivery and targeting: drug-dendrimer interactions and toxicity issues. *J. Pharm. BioAllied Sci.* **2014**, *6*, 139−150.

(22) Gajbhiye, V.; Palanirajan, V. K.; Tekade, R. K.; Jain, N. K. Dendrimers as therapeutic agents: a systematic review. *J. Pharm. Pharmacol.* **2009**, *61*, 989−1003.

(23) Li, Z.; Hu, J.; Yang, L.; Zhang, X.; Liu, X.; Wang, Z.; Li, Y. Integrated POSS-dendrimer nanohybrid materials: current status and future perspective. *Nanoscale* **2020**, *12*, 11395−11415.

(24) Yamamoto, K.; Imaoka, T.; Tanabe, M.; Kambe, T. New Horizon of Nanoparticle and Cluster Catalysis with Dendrimers. *Chem. Rev.* **2020**, *120*, 1397−1437.

(25) Lyu, Z.; Ding, L.; Huang, A. Y. T.; Kao, L.; Peng, L. Poly(amidoamine) dendrimers: covalent and supramolecular synthesis. *Mater. Today Chem.* **2019**, *13*, 34−48.

(26) Caminade, A. M.; Turrin, C. O.; Majoral, J. P. *Phosphorus Dendrimers in Biology and Nanomedicine: Syntheses, Characterization, and Properties*; Jenny Stanford Publishing Pte. Ltd., 2018.

(27) Mignani, S.; El Brahmi, N.; El Kazzouli, S.; Laurent, R.; Sonia Ladeira, S.; Caminade, A.-M.; Pedziwiatr-Werbicka, E.; Szewczyk, E. M.; Bryszewska, M.; Bousmina, M. M.; Cresteil, T.; Majoral, J.-P. Original multivalent gold(III) and dual gold(III)−copper(II) conjugated phosphorus dendrimers as potent antitumoral and antimicrobial agents. *Mol. Pharmaceutics* **2017**, *14*, 4087−4097.

(28) Solassol, J.; Crozet, C.; Perrier, V.; Leclaire, J.; Beranger, F.; Caminade, A. M.; Meunier, B.; Dormont, D.; Majoral, J.-P.; Lehmann, S. Cationic phosphorus-containing dendrimers reduce prion replication both in cell culture and in mice infected with scrapie. *J. Gen. Virol.* **2004**, *85*, 1791−1799.

(29) Wasiak, T.; Marcinkowska, M.; Pieszynski, I.; Zablocka, M.; Caminade, A. M.; Majoral, J. P.; Klajnert-Maculewicz, B. Cationic phosphorus dendrimers and therapy for Alzheimer's disease. *New J. Chem.* **2015**, *39*, 4852−4859.

(30) Blattes, E.; Vercellone, A.; Eutamène, H.; Turrin, C. O.; Théodorou, V.; Majoral, J. P.; Caminade, A. M.; Prandi, J.; Nigou, J.; Puzo, G. Mannodendrimers prevent acute lung inflammation by inhibiting neutrophil recruitment. *Proc. Natl. Acad. Sci. U.S.A.* **2013**, *110*, 8795−8800.

(31) Mignani, S.; El Kazzouli, S.; Bousmina, M.; Majoral, J.-P. Expand classical drug administration ways by emerging routes using dendrimer drug delivery systems: A Concise overview. *Adv. Drug Delivery Rev.* **2013**, *35*, 1316−1330.
(32) Kana, B. D.; Karakousis, P. C.; Parish, T.; Dicke, T. Future target-based drug discovery for tuberculosis? *Tuberculosis* **2014**, *94*, 551−556.
(33) Sabbah, M.; Mendes, V.; Vistal, R. G.; Dias, D. M. G.; Monika Záhorszká, M.; Mikušová, K.; Korduláková, J.; Coyne, A. G.; Blundell, T. L.; Abell, C. Fragment-Based Design of *Mycobacterium tuberculosis* InhA Inhibitors. *J. Med. Chem.* **2020**, *63*, 4749−4761.
(34) Cavero, E.; Zablocka, M.; Caminade, A. M.; Majoral, J. P. Design of Bisphosphonate-terminated Dendrimers. *Eur. J. Org. Chem.* **2010**, *14*, 2759−2767.
(35) Slany, M.; Bardaji, M.; Casanove, M.-J.; Caminade, A.-M.; Majoral, J.-P.; Chaudret, B. Dendrimer Surface Chemistry. Facile Route to Polyphosphines and Their Gold Complexes. *J. Am. Chem. Soc.* **1995**, *117*, 9764−9765.
(36) Launay, N.; Caminade, A. M.; Lahana, R.; Majoral, J. P. A general synthetic strategy for neutral phosphorus-containing dendrimers. *Angew. Chem., Int. Ed.* **1994**, *33*, 1589−1592.
(37) Padié, C.; Maszewska, M.; Majchrzak, K.; Nawrot, B.; Caminade, A.-M.; Majoral, J.-P. Polycationic phosphorus dendrimers: synthesis, characterization, study of cytotoxicity, complexation of DNA, and transfection experiments. *New J. Chem.* **2009**, *33*, 318−326.
(38) Badetti, E.; Caminade, A.-M.; Majoral, J.-P.; Moreno-Mañas, M.; Sebastián, R. M. Palladium(0) Nanoparticles Stabilized by Phosphorus Dendrimers Containing Coordinating 15-Membered Triolefinic Macrocycles in Periphery. *Langmuir* **2008**, *24*, 2090−2101.
(39) Garcia, L.; Roglans, A.; Laurent, R.; Majoral, J.-P.; Pla-Quintana, A.; Caminade, A.-M. Dendritic phosphoramidite ligands for Rh-catalyzed [2+2+2] cycloaddition reactions: unprecedented enhancement of enantiodiscrimination. *Chem. Commun.* **2012**, *48*, 9248−9250.
(40) *Schrödinger Release 2020-2*; Schrödinger, LLC: New York, NY, 2020.
(41) Bochevarov, A. D.; Harder, E.; Hughes, T. F.; Greenwood, J. R.; Braden, D. A.; Philipp, D. M.; Rinaldo, D.; Halls, M. D.; Zhang, J.; Friesner, R. A. Jaguar: A high-performance quantum chemistry software program with strengths in life and materials sciences. *Int. J. Quantum Chem.* **2013**, *113*, 2110−2142.
(42) Bowers, K. J.; Chow, E.; Xu, H.; Dror, R. O.; Eastwood, M. P.; Gregersen, B. A.; Klepeis, J. L.; Kolossvary, I.; Moraes, M. A.; Sacerdoti, F. D.; Salmon, J. K.; Shan, B.; Shaw, D. E. In *Scalable Algorithms for Molecular Dynamics Simulations on Commodity Clusters*, Proceedings of the ACM/IEEE Conference on Supercomputing (SC06), Tampa, Florida, USA, November 11−17, 2006.
(43) Harder, E.; Damm, W.; Maple, J.; Wu, C.; Reboul, M.; Xiang, J. Y.; Wang, L.; Lupyan, D.; Dahlgren, M. K.; Knight, J. L.; Kaus, J. W.; Cerutti, D. S.; Krilov, G.; Jorgensen, W. L.; Abel, R.; Friesner, R. A. OPLS3: A Force Field Providing Broad Coverage of Drug-like Small Molecules and Proteins. *J. Chem. Theory Comput.* **2016**, *12*, 281−296.
(44) Swinney, D. C.; Anthony, J. How were new medicines discovered? *Nat. Rev. Drug Discovery* **2011**, *10*, 507−519.
(45) Mignani, S.; El Kazzouli, S.; Bousmina, M. M.; Majoral, J.-P. Dendrimer space concept for innovative nanomedicine: a futuristic vision for medicinal chemistry. *Prog. Polym. Sci.* **2013**, *38*, 993−1008.
(46) Schirle, M.; Jenkins, J. L. Identifying compound efficacy targets in phenotypic drug discovery. *Drug Discovery Today* **2016**, *21*, 82−89.
(47) Payne, D. J.; Gwynn, M. N.; Holmes, D. J.; Pompliano, D. L. Drugs for bad bugs: confronting the challenges of antibacterial discovery. *Nat. Rev. Drug Discovery* **2007**, *6*, 29−40.
(48) Mignani, S.; Rodrigues, J.; Roy, R.; Shi, X.; Cena, V.; El Kazzouli, S.; Majoral, J.-P. Exploration of biomedical dendrimer space based on in-vivo physicochemical parameters: Key factor analysis (Part 2). *Drug Discovery Today* **2019**, *24*, 1184−1192.
(49) Mignani, S.; Rodrigues, J.; Roy, R.; Shi, X.; Ceña, V.; El Kazzouli, S.; Majoral, J.-P. Exploration of biomedical dendrimer space based on in-vitro physicochemical parameters: key factor analysis (Part 1). *Drug Discovery Today* **2019**, *24*, 1176−1183.
(50) Laborde, J.; Deraeve, C.; Bernardes-Génisson, V. Update of Antitubercular Prodrugs from a Molecular Perspective: Mechanisms of Action, Bioactivation Pathways, and Associated Resistance. *ChemMedChem* **2017**, *20*, 1657−1676.
(51) Iacobino, A.; Fattorini, L.; Giannoni, F. Drug-Resistant Tuberculosis 2020: Where We Stand. *Appl. Sci.* **2020**, *10*, No. 2153.

https://doi.org/10.1021/acs.biomac.1c00355
Biomacromolecules 2021, 22, 2659−2675